Jordan-Wigner approach to dynamic correlations in spin ladders

Tamara S. Nunner* and Thilo Kopp
EP VI, Universität Augsburg, 86135 Augsburg, Germany
(Received 5 August 2003; revised manuscript received 22 December 2003; published 22 March 2004)

We present a method for studying the excitations of low-dimensional quantum spin systems based on the Jordan-Wigner transformation. Using an extended random-phase approximation (RPA) scheme we calculate the correlation function of neighboring spin flips for the one-dimensional spin-1/2 chain which well approximates the optical conductivity of Sr_2CuO_3. We analyze several possible generalizations of the Jordan-Wigner approach to the two-leg spin-1/2 ladder. On the mean-field level the most accurate results are obtained when the spin operators are numbered in a meanderlike sequence. Calculation of the optical conductivity based on an extended RPA scheme for the meander-path approach yields very good agreement with a previous density matrix renormalization group evaluation. For polarization along the legs higher-order correlations are important to explain the weight of high-energy continuum excitations and we estimate the contribution of 4- and 6-fermion processes.

DOI: 10.1103/PhysRevB.69.104419 PACS number(s): 75.10.Jm, 75.40.Gb, 75.40.Mg, 74.72.Jt

I. INTRODUCTION

Due to the presence of strong quantum fluctuations, low-dimensional spin systems show very complex behavior and provide a challenge for theoretical treatments. In this context, $S=\frac{1}{2}$ Heisenberg spin ladders are especially interesting because they represent an interjacent system, in between the antiferromagnetic $S=\frac{1}{2}$ Heisenberg chain and the two-dimensional antiferromagnetic Heisenberg model. Early on, these spin ladders were considered as systems which display a dimensional crossover between one and two dimensions.[1] However, spin ladders do not constitute a ''smooth crossover'' because even-leg spin ladders acquire a spin liquid ground state and finite spin gap.[2,3] This is in contrast to the critical systems, the $S=\frac{1}{2}$ chain and the odd-leg ladders, which exhibit algebraically decaying spin correlations, and it is in contrast to the 2D antiferromagnetic Heisenberg model, for which a long-range Néel-ordered ground state was established.[4] In a field-theoretical mapping of the low-energy modes on an O(3) nonlinear σ model this even-odd effect with the number of legs results from the addition of a topological term. The term was demonstrated to be zero for even-leg ladders and the two-dimensional Heisenberg model and finite for odd-leg ladders as well as the $S=\frac{1}{2}$ chain.[5–8] Correspondingly the system is gapless for odd-leg ladders and gapful for even-leg ladders whereby the gap decreases exponentially with the number of legs.

In this paper we will focus on the antiferromagnetic two-leg $S=\frac{1}{2}$ ladders. The two-leg ladder can be approached conceptionally from the limit of strong coupling $J_\perp$ along the rungs.[9–14] Then the elementary excitations may be considered as excitations of rung triplets which propagate throughout the ladder due to the finite leg coupling J. For small coupling $J_\perp/J$, a more natural description would seem to be in terms of the spinon excitations of the isolated legs. However, the excitations of the two-leg spin ladders cannot be constructed perturbatively from spinons of the chains since the rung coupling is a relevant perturbation. The spinons are confined and have to form bound states on the ladder.[15,16]

Of particular interest is the intermediate coupling regime $J\approx J_\perp$, as this case is related to the two-dimensional systems. It is also realized in cuprate spin ladder compounds,[17] which are of interest due to their affinity to the cuprate high-T_c superconductors. Recently, the spin-singlet excitation spectrum of the spin ladder compound $(La,Ca)_{14}Cu_{24}O_{41}$ has been investigated in midinfrared (MIR) absorption experiments.[18] In the optical conductivity $\sigma(\omega)$, magnetic excitations can be observed from the simultaneous excitation of a phonon which generates a finite dipole moment for the considered field polarization, a mechanism introduced by Lorenzana and Sawatzky for the undoped high-T_c cuprates.[25] The phonon, assisting the magnetic excitation, takes up momentum which implies that spin excitations with all wave vectors in the Brillouin zone enter $\sigma(\omega)$. The relative spectral weight for the different wave vectors is determined by the proper form factor of the considered phonon.[19] Due to weak magnon-phonon interaction the propagation of the phonon is assumed to decouple from the spin excitations. Consequently, the dynamical response is evaluated with a spin-only model Hamiltonian, and the phonons account merely for the appropriate wave-vector summation and frequency shift. Indeed, we were able to confirm through a dynamical DMRG evaluation[20] that a nearest-neighbor Heisenberg model with an additional cyclic spin-exchange term is sufficient for the two-leg spin ladders: it reproduces remarkably well the observed MIR optical conductivity within this scheme of phonon-assisted magnetic excitations.

In order to gain control over the spin excitations and to better identify the observed MIR resonances an analytical approach is required which—despite the necessary approximations to make the calculation feasible—is still adequate to retrieve the considered excitations of the spin liquid state. An analytical approach which helped to identify the observed resonances as spin-singlet dispersive bound states and continuum excitations was presented by us along with the experimental data of Windt *et al.*[18] We proposed to use a one-dimensional fermionic representation of the spin operators which is generated through a Jordan-Wigner transformation.[21,22] Treatments of the spin ladder based on the Jordan-Wigner transformation along a one-dimensional path have been suggested before.[23,24] The advantage of this fermionic representation over many bosonic representations

is the absence of constraints or the restriction to a $1/S$ expansion. However, the spin operator in terms of the ''Jordan-Wigner fermions'' becomes a nonlocal operator with a long-ranged phase factor, necessary to fulfill the spin commutation relations. Conveniently, the long-range part of the phase cancels in the Hamiltonian as well as in the spin correlations which enter the optical conductivity. For the one-dimensional spin chain the fermionic Hamiltonian is then composed of a bilinear, kinetic part which presents the XY interaction of nearest-neighbor spins and a density-density interaction which presents the Ising part of the interaction of nearest-neighbor spins. For the spin ladder this Hamiltonian is extended by interaction terms with 4- and 6-fermionic operators which are introduced through the exchange of spins on sites which are nearest neighbor in the lattice but are not adjacent along the one-dimensional path through the lattice. These interactions originate from phase operators which are not exactly matched as for adjacent sites on the path.

In order to investigate the dynamical response for the full spectrum, we apply the random-phase approximation (RPA), a standard perturbative approach. For the considered fermionic model, the strength of the interaction is set by the same scale as the kinetic term and, correspondingly, RPA is not controlled by a small parameter (for $J \approx J_\perp$). However, we will compare the results with those of the dynamical density matrix renormalization group (DMRG) and thereby confirm the validity of the approach.

In the present paper, we discuss this approach to a spin-1/2 chain and then in detail to two-leg ladders. In Sec. II we start with the simpler case of a spin-1/2 chain in order to introduce our approximation scheme for the Jordan-Wigner fermions. We calculate $\sigma(\omega)$ for the 1D-spin chain in RPA and compare it with the optical conductivity of Sr_2CuO_3 measured by Suzuura *et al.*[26] In Sec. III A we generalize the Jordan-Wigner treatment to the two-leg spin ladder. A proper treatment of the phase factor turns out to be essential and we find that an approach based on a meander path yields the most accurate mean-field description. As this approach causes a slight dimerization of the spin ladder, the origin for this behavior and its consequences will be analyzed. In Sec. III B we present an RPA scheme for the evaluation of dynamic correlation functions, which is based on the meander-path formulation of the Jordan-Wigner transformation. We use this scheme to calculate the optical conductivity $\sigma(\omega)$ of the two-leg ladder and check the reliability of our approach by comparing it with a DMRG correction-vector[27] evaluation.

II. JORDAN-WIGNER TRANSFORMATION FOR THE 1D SPIN-1/2 CHAIN

First we recall the Jordan-Wigner transformation for the 1D spin-1/2 chain and introduce our approximation scheme. The fact that we find good agreement with the spinon evaluation for the 1D spin chain inspired us to extend the approach to two-leg spin ladders as will be discussed in Sec. III.

Since spin operators do not obey canonical commutation relations, it is convenient to transform them either into bosonic or fermionic operators, in order to permit the application of standard diagrammatic perturbation theory. With any mapping, however, the algebra of the original spin operators has to be preserved. In the Jordan-Wigner transformation this is provided by rewriting the spin operators as fermionic operators with a long-ranged phase factor

$$S_i^- = c_i e^{i\Phi_i}, \quad \Phi_i = \pi \sum_{j<i} c_j^\dagger c_j, \quad S_i^z = \left(c_i^\dagger c_i - \frac{1}{2} \right), \quad (1)$$

which transforms the 1D antiferromagnetic Heisenberg Hamiltonian ($J>0$) to the fermionic Hamiltonian

$$H = J \sum_i \left\{ \frac{1}{2} (c_i^\dagger c_{i+1} + c_{i+1}^\dagger c_i) + \left(c_i^\dagger c_i - \frac{1}{2} \right) \left(c_{i+1}^\dagger c_{i+1} - \frac{1}{2} \right) \right\}. \quad (2)$$

The first term in Eq. (2) corresponds to the XY part of the original Heisenberg Hamiltonian. In the fermionic representation it acts as a nearest-neighbor hopping. The second term, which originates from the Ising term of the original Heisenberg Hamiltonian, introduces a nearest-neighbor density-density interaction among the fermions. The chemical potential of the fermions corresponds to a magnetic field for the spin system. For the paramagnetic state, the chemical potential has to constrain the particle number to the respective particle number density of a half-filled band.

The fermionic Hamiltonian does not include operator products with site index distances of more than one lattice spacing because in products of neighboring spins the phase factors drop out. This is due to the fact that the fermion operator c_i commutes with the phase ϕ_i of the same site ($[c_i, \phi_i] = 0$). Correspondingly, the representation is particularly useful for models with nearest-neighbor exchange interactions. However even so, not all dynamical correlation functions can be evaluated without further approximations or elaborate techniques: for example, the transverse spin correlation generates ''long-range'' phase factors with a summation over a major fraction of the lattice sites. McCoy *et al.* devised a scheme[28] with which they succeeded to calculate the transverse response in the XY model (see also the approach by Luther and Peschel[29]). For the longitudinal spin response and the optical conductivity, a nearest-neighbor spin-singlet response, where the phase factors drop out, these sophisticated techniques are not required and one may evaluate the correlators with standard diagrammatic techniques.

A. Mean-field treatment—$d=1$

Following Wang,[30] the Ising interaction can be treated in mean-field approximation (MFA) by introducing a nearest-neighbor ''covalent bonding'' of the Jordan-Wigner fermions $\chi = \langle c_i^\dagger c_{i+1} \rangle$:

$$H_{MF} = J \sum_k (1 - 2\chi) \cos k c_k^\dagger c_k \quad \text{with} \quad \chi = -\frac{1}{\pi}. \quad (3)$$

The ground state of the Heisenberg model has no net magnetization $\langle S_i^z \rangle = 0$. Within the fermionic representation this

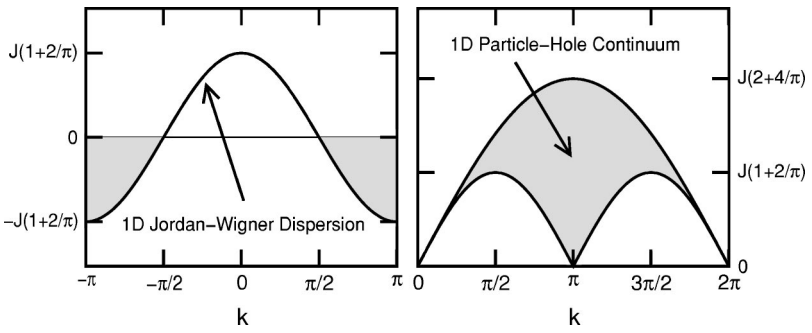

FIG. 1. Left panel: mean-field dispersion for the Jordan-Wigner fermions in $d=1$, gray shading denotes the filling in the ground state. Right panel: continuum of Jordan-Wigner particle-hole excitations in $d=1$.

implies that the fermion system is at half filling $\langle c_i^\dagger c_i\rangle=\frac{1}{2}$. The ground state is obtained by filling up all negative-energy states. This leads to a Fermi surface at wave vectors $k_f=\pm\pi/2$, as displayed in Fig. 1. Adding/removing a fermion to the system corresponds to $S_z=\pm 1$ excitations, $S_z=0$ excitations can be realized by particle-hole excitations. The particle-hole continuum of the Jordan-Wigner fermions, displayed in Fig. 1, is very similar to the two-spinon continuum.[31] The upper cutoff of the Jordan-Wigner particle-hole continuum is at $(2+4/\pi)J\approx 3.27J$ and therefore close to πJ which is the maximum energy for two spinons.

B. RPA for optical conductivity—$d=1$

Spin excitations can be observed in the midinfrared range of the optical conductivity $\sigma(\omega)$ due to the simultaneous excitation of a phonon.[25] The optical conductivity of the 1D spin-chain compound Sr_2CuO_3[26] has been nearly perfectly reproduced by Lorenzana and Eder[32] using an ansatz based on numerical results in finite chains, sum rules, and Bethe ansatz results. Originally, a similar procedure was suggested by Müller *et al.*[33] for the evaluation of the dynamic structure factor $S(k,\omega)$, taking advantage of the observation that the two-spinon contribution is the class of Bethe-ansatz solutions which carries most of the weight of the continuum excitations. Only recently, it has been possible to determine the two-spinon contribution to $S(k,\omega)$ exactly.[34,35]

For the optical conductivity, however, an exact expression of the two-spinon contribution is not yet available. Nevertheless, the evaluation of Lorenzana and Eder,[32] which so convincingly reproduces the shape of the cusplike, wide structure in $\sigma(\omega)$, confirms that the observed resonance indeed results from two-spinon excitations of the nearest-neighbor Heisenberg model. This motivated us to use the established $\sigma(\omega)$ of the 1D spin chain as a reference and to check for the quality of the results of our analytical Jordan-Wigner approach. We calculate the two-particle correlation function $\sigma(\omega)$ within an extended RPA scheme, i.e., by summing up bubble and ladder diagrams, and compare our result with the experimental optical conductivity of Sr_2CuO_3.[26]

For the one-dimensional spin chain the phonon-assisted magnetic contribution to the optical conductivity is given by[25,32]

$$\sigma(\omega)\sim -16\,\omega\sum_p \sin^4\left(\frac{p}{2}\right)\mathrm{Im}\langle\langle \delta B_{-p};\delta B_p\rangle\rangle_{(\omega-\omega_{ph})}. \tag{4}$$

The spin-flip operator δB_p is expressed in MFA by

$$\delta B_p=\frac{1}{N}\sum_i e^{ipr_i}(\mathbf{S}_i\mathbf{S}_{i+1}-\langle\mathbf{S}_i\mathbf{S}_{i+1}\rangle)$$
$$\approx e^{-ip/2}\frac{1}{N}\sum_k (1-2\chi)\cos\left(k+\frac{p}{2}\right)c_k^\dagger c_{k+p}. \tag{5}$$

This yields for the dynamic spin-flip correlation function in Zubarev notation

$$\langle\langle \delta B_{-p};\delta B_p\rangle\rangle=\frac{1}{N}\sum_p (1-2\chi)^2\Big\{\cos^2\frac{p}{2}B^{(1,1)}(p,\omega)$$
$$-\cos\frac{p}{2}\sin\frac{p}{2}[B^{(1,2)}(p,\omega)+B^{(2,1)}(p,\omega)]$$
$$+\sin^2\frac{p}{2}B^{(2,2)}(p,\omega)\Big\}, \tag{6}$$

with particle-hole propagators

$$B^{(\mu,\nu)}(p,\omega)=\sum_{k,q} f_k^\mu f_q^\nu\langle\langle c_k^\dagger c_{k+p};c_{q+p}^\dagger c_q\rangle\rangle \tag{7}$$

and the following form factors:

$$f_k^0=1,\quad f_k^1=\cos k,\quad f_k^2=\sin k. \tag{8}$$

Summing all particle-hole scattering processes, as illustrated in Fig. 2 in diagrammatic terms, a simple expression for the renormalized particle-hole propagator can be obtained

$$B^{(\mu,\nu)}(p,\omega)=b^{(\mu,\nu)}(p,\omega)+2J\cos p\, b^{(\mu,0)}(p,\omega)B^{(0,\nu)}(p,\omega)$$
$$-2J\, b^{(\mu,1)}(p,\omega)B^{(1,\nu)}(p,\omega)$$
$$-2J\, b^{(\mu,2)}(p,\omega)B^{(2,\nu)}(p,\omega), \tag{9}$$

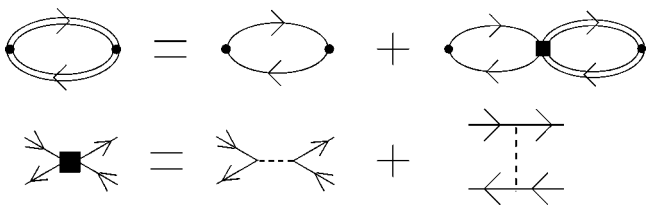

FIG. 2. Diagrammatic scheme for the extended RPA treatment of Jordan-Wigner fermions in Eq. (9).

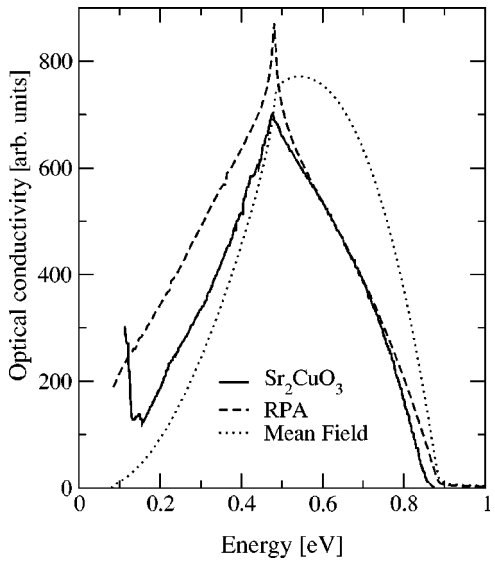

FIG. 3. $\sigma(\omega)$ obtained with Jordan-Wigner fermions in comparison with the experimental optical conductivity of Sr_2CuO_3 (solid line), taken from Suzuura *et al.* (Ref. 26). Dotted line—mean-field approximation, dashed line—RPA approximation. Following Lorenzana and Eder (Ref. 32) we have subtracted the same linear background from the experimental data and we have used the same value for the exchange coupling $J=0.246$ eV and for the phonon frequency $\omega_{ph}=0.08$ eV.

where the noninteracting particle-hole propagators are given by

$$b^{(\mu,\nu)}(p,\omega)=\frac{1}{N}\sum_k f_k^\mu f_k^\nu\left\{\frac{(1-\langle n_{k+p}\rangle)\langle n_k\rangle}{\omega+\epsilon_k-\epsilon_{p+k}+i0^+}-\frac{(1-\langle n_k\rangle)\langle n_{p+k}\rangle}{\omega+\epsilon_k-\epsilon_{p+k}-i0^+}\right\}. \quad (10)$$

Evaluation of these equations determines $\sigma(\omega)$ which is shown in Fig. 3 in comparison with the experimental spectrum of Sr_2CuO_3 taken from Suzuura *et al.*[26]

A simple analysis of the experimental line shape of Sr_2CuO_3 based on Jordan-Wigner fermions has already been discussed by Suzuura *et al.*[26] in combination with the experimental results. However, they restricted the evaluation to the *XY* model which corresponds to our mean-field evaluation apart from a renormalization of the energy scale by a factor of $1+2/\pi$ in Eq. (3). We find that it is important to treat the two-particle correlation function $\sigma(\omega)$ at least within RPA. The resonance is shifted to lower energies compared to the mean-field approximation. In addition we observe a cusp at $\omega=J(1+2/\pi)$ as a precursor of the logarithmic singularity found by Lorenzana and Eder.[32] Although the RPA slightly overestimates the interaction strength which results in shifting too much spectral weight to energies below the cusp, it favorably reproduces the experimental $\sigma(\omega)$ with respect to the position of the cusp and its high-energy side.

The interpretation of the absorption spectrum is as follows: On the mean-field level a Van Hove singularity at the position of the band edge of the Jordan-Wigner fermions [at $(1+2/\pi)J$] is generated. The corresponding kink in the spectral density is replaced by the sharp cusp on the RPA level, as seen in Fig. 3. The interaction strength in the RPA equation [Eq. (9)] is not sufficiently strong to produce a bound state well below the continuum. Only a precursor to the bound state, which is a resonance along the lower edge of the particle-hole continuum, is formed (the lower curve on the right panel of Fig. 1). Thereby it takes spectral weight from the rest of the continuum, as seen in Fig. 3 from the comparison of the MFA and RPA results: the high-energy continuum weight is partly moved to the lower edge of the continuum, with highest weight at $k\simeq\pi/2$, responsible for the formation of the cusp. On the RPA level, this effect is slightly overestimated. Higher-order scattering processes of the Jordan-Wigner fermions should partly compensate this spectral shift. However, the investigation of the corresponding vertex corrections is beyond the scope of this paper. A correction of the RPA line shape in Fig. 3 does not necessarily introduce new aspects for the interpretation of the spin correlations on the chain.

III. JORDAN-WIGNER TRANSFORMATION FOR THE TWO-LEG $S=\frac{1}{2}$ LADDER

Motivated by the convincing results of the Jordan-Wigner fermion treatment for the Heisenberg $S=\frac{1}{2}$ chain we ''slightly increase'' the dimensionality and extend the approach to the nearest-neighbor Heisenberg two-leg $S=\frac{1}{2}$ ladder:

$$H=J_\perp\sum_i \mathbf{S}_{i,1}\mathbf{S}_{i,2}+J\sum_i(\mathbf{S}_{i,1}\mathbf{S}_{i+1,1}+\mathbf{S}_{i,2}\mathbf{S}_{i+1,2}), \quad (11)$$

where $J_\perp$ is the exchange coupling along the rungs, J the coupling along the legs, i refers to the site index along the legs, and the subscripts 1,2 label the two different legs.

Generalizations of the Jordan-Wigner transformation to higher dimensions have been suggested[36,37] and may be adopted for spin ladders. The phase factor, however, the proper treatment of which is essential as demonstrated in Sec. III A 1, can be treated most accurately using the one-dimensional Jordan-Wigner transformation, i.e., by arranging all spins in a one-dimensional sequence. With this scheme the range of the interaction terms can be controlled through a convenient choice of a path which covers all sites. The application of a two-dimensional representation to the spin ladders, on the other hand, would generate long-range interaction terms in the Hamiltonian.

Possible path configurations through a two-leg ladder are shown in Fig. 4. The path displayed in Fig. 4(a) is obviously very close to the one-dimensional situation. As a consequence the rung interaction is difficult to treat in this representation because every product of neighboring rung spins contains a number of phase factors, which diverges with the length of the spin ladder. The rung coupling, however, is a relevant perturbation since the excitation spectrum of a two-leg ladder remains gapped for all coupling ratios $J_\perp/J$. Therefore a path which passes through all the rungs should be more suitable. Possible realizations are a zigzag path[24]

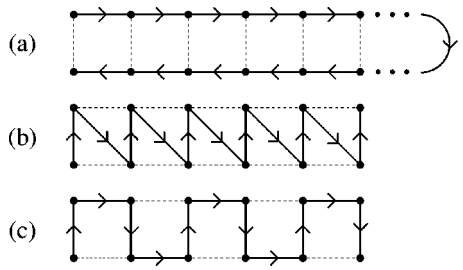

FIG. 4. Possible path configurations for a two-leg ladder.

and a meander path,[23] displayed in Figs. 4(b) and 4(c), respectively. Although the zigzag path appears simpler and more symmetric at first sight, only a mean-field treatment (analogous to the preceding section) based on the meander path yields a reasonable description of the one-triplet excitations and only the meander path correctly reproduces the strong-coupling limit of the one-triplet dispersion $\epsilon_k = J_\perp + J\cos k$ for $J_\perp/J \gg 1$ (see Sec. III A 2).

A. Meander path

Following Dai and Su[23] we divide the ladder into two sublattices as indicated in Fig. 5. Introducing two species of spinless fermions α_i and β_i, the spin operators on the two sublattices transform as

$$S^+_{i,\alpha} = \alpha_i^\dagger \exp\left[i\pi \sum_{j<i} (\alpha_j^\dagger \alpha_j + \beta_j^\dagger \beta_j) \right],$$

$$S^+_{i,\beta} = \beta_i^\dagger \exp\left[i\pi \sum_{j<i} (\alpha_j^\dagger \alpha_j + \beta_j^\dagger \beta_j) \right] e^{i\pi \alpha_i^\dagger \alpha_i}, \qquad (12)$$

where the summation in the phase factor is along the meander path. For products of spin operators, which are not successive along the meander path, e.g., $S^+_{i,\alpha} S^-_{i+1,\beta} + S^-_{i,\alpha} S^+_{i+1,\beta}$, the phases corresponding to intermediate sites along the meander path do not cancel. This is different from the one-dimensional situation where all nearest-neighbor spin operators are also successive along the path. Using transformation (12) the Heisenberg Hamiltonian of Eq. (11) becomes

$$\begin{aligned} H = J_\perp \sum_i & \left\{ \frac{1}{2}(\alpha_i^\dagger \beta_i + \beta_i^\dagger \alpha_i) + \left(\alpha_i^\dagger \alpha_i - \frac{1}{2} \right) \left(\beta_i^\dagger \beta_i - \frac{1}{2} \right) \right\} \\ & + J \sum_i \left\{ \frac{1}{2} [\beta_i^\dagger \alpha_{i+1} + \alpha_i^\dagger \beta_{i+1} e^{i\pi(n_{\beta_i} + n_{\alpha_{i+1}})} + \text{H.c.}] \right. \\ & + \left(\alpha_i^\dagger \alpha_i - \frac{1}{2} \right) \left(\beta_{i+1}^\dagger \beta_{i+1} - \frac{1}{2} \right) \\ & \left. + \left(\alpha_{i+1}^\dagger \alpha_{i+1} - \frac{1}{2} \right) \left(\beta_i^\dagger \beta_i - \frac{1}{2} \right) \right\}. \end{aligned} \qquad (13)$$

Unfortunately the phase factor $e^{i\pi(n_{\beta_i} + n_{\alpha_{i+1}})}$ from spin products of nonsuccessive sites cannot be treated exactly. Dai and Su have replaced this phase factor by its average value. This treatment, however, can be improved in a systematic way by rewriting the phase factor:

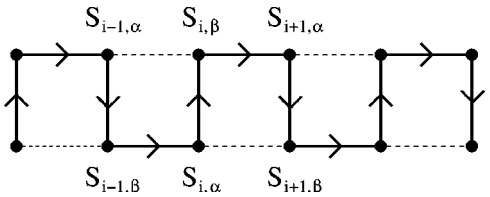

FIG. 5. Sublattice structure for the meander path.

$$e^{i\pi(n_{\beta_i} + n_{\alpha_{i+1}})} = (1 - 2\beta_i^\dagger \beta_i)(1 - 2\alpha_{i+1}^\dagger \alpha_{i+1}) \qquad (14)$$

and reinserting this exact expansion into Hamiltonian (13). In this way we obtain additional interaction terms containing 4- and 6-fermion operators which we now treat on the same footing as the Ising-interaction terms.

Following the mean-field treatment for the spin chain we consider all possible nearest-neighbor bond amplitudes:

$$\chi_0 = \langle \beta_i^\dagger \alpha_i \rangle, \quad \chi_1 = \langle \beta_i^\dagger \alpha_{i+1} \rangle, \quad \chi_2 = \langle \alpha_i^\dagger \beta_{i+1} \rangle. \qquad (15)$$

Taking into account all possible contractions of the 4- and 6-fermion operator terms we arrive at the following mean-field Hamiltonian:

$$H_{MF} = \sum_k (\gamma_k \alpha_k^\dagger \beta_k + \text{H.c.}), \qquad (16)$$

with

$$\begin{aligned} \gamma_k = & J_\perp(\tfrac{1}{2} - \chi_0) + 4J\chi_0\chi_1 \\ & + J\cos k(\tfrac{1}{2} + 2\chi_0^2 - 4\chi_1\chi_2 - \chi_1 - \chi_2 - 2\chi_1^2) \\ & + iJ\sin k(\tfrac{1}{2} + 2\chi_0^2 - 4\chi_1\chi_2 - \chi_1 + \chi_2 + 2\chi_1^2). \end{aligned} \qquad (17)$$

This expression has already been simplified using that χ_0, χ_1, and χ_2 turn out to be real. The above Hamiltonian can easily be diagonalized

$$H_{MF} = \sum_k \epsilon_k (\tilde{\alpha}_k^\dagger \tilde{\alpha}_k - \tilde{\beta}_k^\dagger \tilde{\beta}_k) \quad \text{with} \quad \epsilon_k = |\gamma_k|, \qquad (18)$$

using

$$\alpha_k = \frac{1}{\sqrt{2}} u_k (\tilde{\alpha}_k + \tilde{\beta}_k), \quad \beta_k = \frac{1}{\sqrt{2}} v_k (\tilde{\alpha}_k - \tilde{\beta}_k),$$

$$u_k = v_k^* = e^{i\phi_k/2}, \quad \gamma_k = |\gamma_k| e^{i\phi_k}. \qquad (19)$$

The bond amplitudes can then be calculated via

$$\chi_0 = -\frac{1}{2N} \sum_k u_k^2, \quad \chi_1 = -\frac{1}{2N} \sum_k u_k^2 e^{-ik},$$

$$\chi_2 = -\frac{1}{2N} \sum_k v_k^2 e^{-ik}, \qquad (20)$$

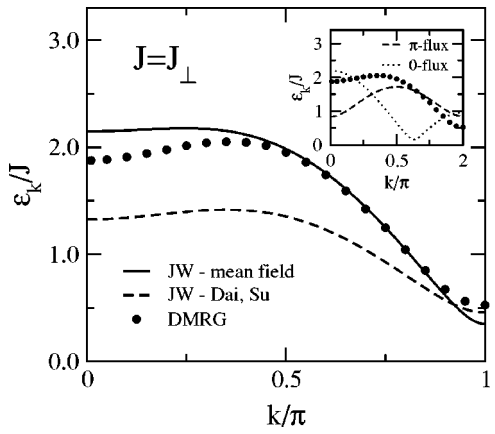

FIG. 6. Dispersion for the isotropic ladder $J=J_\perp$. Solid line—mean-field dispersion for Jordan-Wigner fermions; dashed line—dispersion obtained by averaging the phase factor analogous to the treatment by Dai and Su (Ref. 23); circles—one-triplet dispersion obtained with DMRG for a $N=80$ site ladder (Ref. 20). Inset: dispersion obtained for a flux-phase approximation of the phase factor with 0 flux (dotted line) and π flux (dashed line) through a plaquette.

and for the isotropic ladder, i.e., $J=J_\perp$, we obtain $\chi_0=-0.3617$, $\chi_1=-0.2679$, and $\chi_2=0.1777$.

The ground state of the two-leg ladder, which has no net magnetization, consists of a filled $\tilde{\beta}_k$ band and an empty $\tilde{\alpha}_k$ band. A spin-1 excitation corresponds to adding an $\tilde{\alpha}_k$ fermion to the system. Therefore the dispersion of the one-triplet excitation is simply given by the dispersion ϵ_k of the $\tilde{\alpha}_k$ band. The mean-field dispersion ϵ_k for the isotropic ladder, $J=J_\perp$, is displayed in Fig. 6 in comparison with the dispersion for an $N=80$ site ladder obtained by DMRG.[20] For momenta between $k\approx 0.5\pi-0.9\pi$ we find nearly perfect agreement with the DMRG results. Only the spin gap, which corresponds to $\epsilon_{k=\pi}$ is slightly too small and the energy for momenta $k<\pi/2$ is somewhat overestimated. Still our mean-field treatment even reproduces a dip for small momenta, which is a precursor of the symmetric (with respect to $k=\pi/2$) spinon dispersion of the spin chain. It has not been possible to attain this dispersion dip for the isotropic two-leg ladder within a mean-field treatment of the bosonic bond-operator representation of elementary rung triplets.[10,12]

1. Role of the phase factor

To demonstrate the improvement of our mean-field evaluation with respect to the mean-field treatment by Dai and Su,[23] who replaced the phase factor by its expectation value, we have added their dispersion in Fig. 6. Qualitatively it is very similar to our mean-field dispersion. Its magnitude, however, is by a factor of about 1.5 too small over a large section of the Brillouin zone. Therefore we conclude that an adequate treatment of the phase factor is very important and it is necessary to go beyond a scheme in which the phase factor is replaced by its average value.

The importance of the "phase factor" can be conceived also in the following way. The phase factor $e^{i\pi(n_{\beta_i}+n_{\alpha_{i+1}})}$ in Hamiltonian (13) was generated by products of spin operators with site labels not in sequence along the one-dimensional meander path. As the "matrix elements" of the phase operator are ± 1 one might speculate to find a reasonable mean-field result by replacing the operator uniformly by ± 1. This corresponds to a flux phase treatment of the phase factor, where the flux through a plaquette is chosen to be 0 and π, respectively. Applying the same kind of mean-field treatment as before one obtains $\epsilon_k=|\gamma_k|$ for the mean-field dispersion, where

$$\gamma_k=J_\perp(\tfrac{1}{2}-\chi_0)+J\cos k(1-\chi_1-\chi_2)+iJ\sin k(\chi_2-\chi_1)$$

corresponds to zero flux and

$$\gamma_k=J_\perp(\tfrac{1}{2}-\chi_0)-J\cos k(\chi_1+\chi_2)+iJ\sin k(1-\chi_1+\chi_2)$$

to a π-flux phase. The resulting dispersions for the zero-flux phase (dotted line) and the π-flux phase (dashed line) are displayed in the inset of Fig. 6 in comparison with the DMRG results for an $N=80$ site ladder. Note that the zero-flux phase corresponds to simply replacing the spin operators $S^{+/-}_{\alpha,\beta}$ by fermionic operators $\alpha^\dagger/\alpha$ or $\beta^\dagger/\beta$. The π-flux phase, therefore, is the first correction to the fermionic character of the spin operators and improves the mean-field dispersion notably.

Still, this replacement by a flux phase obviously shows poor agreement with the DMRG dispersion. The mean-field evaluation of the phase factor (dashed line, main panel), as has been proposed by Dai and Su,[23] improves the form of the dispersion at least qualitatively. For a reasonable quantitative agreement with the exact dispersion, however, it is necessary to consider also the correlations related to the phase factor, which are included within our mean-field treatment of the meander path (solid line, main panel). Our mean-field treatment also corresponds to a π-flux state of the spinless fermions, as the product of the bond amplitudes around a plaquette is negative. This π-flux phase, however, is different from the one discussed above, where by construction the complete phase factor is replaced by a flux π.

2. Strong-coupling limit

In the strong-coupling limit our approach reproduces the correct strong-coupling form for the one-triplet dispersion $\epsilon_k=J_\perp+J\cos k$. Expanding with respect to the rung-dimer limit we obtain the following.

Zeroth order $(J/J_\perp)^0$. For $J=0$ the off-diagonal part of the mean-field Hamiltonian (16) reduces to

$$\gamma_k=J_\perp(\tfrac{1}{2}-\chi_0). \tag{21}$$

The resulting Hamiltonian can be diagonalized easily using $u_k=v_k=1$ in Eq. (19) which yields for the nearest-neighbor bond amplitudes, Eq. (20), $\chi_0=-1/2$, $\chi_1=0$, and $\chi_2=0$. This is the limit of rung dimers and the correct value for the energy of a single rung-triplet excitation is obtained as

$$\epsilon_k=|\gamma_k|=J_\perp. \tag{22}$$

First order $(J/J_\perp)^1$. Resubstituting the zeroth-order bond amplitudes in Eq. (17) yields $\gamma_k=J_\perp+J(\cos k+i\sin k)$. Ex-

panding the resulting dispersion to first order in $J/J_\perp$ one obtains the correct strong-coupling limit

$$\epsilon_k = |\gamma_k| = J_\perp \sqrt{1 + 2\frac{J}{J_\perp}\cos k + \left(\frac{J}{J_\perp}\right)^2} \approx J_\perp + J\cos k. \tag{23}$$

This expression contains already all terms to order $J/J_\perp$. This can be easily seen when the above results are inserted into Eq. (20) for the bond amplitudes. To order $J/J_\perp$ one obtains for the diagonalization transformation $u_k = \gamma_k/|\gamma_k| \approx 1 + iJ/J_\perp \sin k$ and consequently for the bond amplitudes $\chi_0 = -1/2$ and $\chi_1 = -\chi_2 = J/(4J_\perp)$. Whereas χ_0 remains unchanged, χ_1 and χ_2 are proportional to $J/J_\perp$ and therefore they contribute to γ_k and ϵ_k only in second order.

3. Symmetry properties

Comparing the fermionic Hamiltonian, Eq. (13), with the original spin Hamiltonian, Eq. (11), one observes that the new fermionic operators α_i and β_i do not conserve all the symmetries of the original spin operators $\mathbf{S}_{i,1}$, $\mathbf{S}_{i,2}$. The sublattice structure underlying the meander path, see Fig. 5, restricts the translational symmetry of the fermions to translations of an even number of sites. Nevertheless, neighboring spin correlations $\langle S^\dagger_{i,\alpha} S^-_{i+1,\beta}\rangle = \langle \alpha^\dagger_i \beta_{i+1}\rangle$ and $\langle S^\dagger_{i,\beta} S^-_{i+1,\alpha}\rangle = \langle \beta^\dagger_i e^{i\pi(\alpha^\dagger_i\alpha_i + \beta^\dagger_i\beta_i)}\alpha_{i+1}\rangle$ should be equal in an exact treatment, because the Hamiltonians themselves are equivalent in the sense that all matrix elements within the considered Fock space are identical. In a mean-field evaluation, however, this equivalence cannot be enforced, because the mean-field evaluation is a variational scheme based on two-particle expectation values, whereas the implementation of this symmetry would require correlations of four particles. In order to resolve this inconsistency, one either has to introduce two-site cluster operators consisting of several fermions or one should choose a more symmetric fermionic representation. In the former case, one would have to work with nonlocal operators which do not obey canonical commutation relations and, consequently, the merits of the fermionization would be lost. The second possibility of choosing a more symmetric fermionic representation will be investigated in Appendix A. It turns out, however, that the meander-path representation is still the most favorable choice, because it allows the best treatment of spin correlations along the legs. Therefore it is intriguing to explore the symmetry behavior of the meander-path model and its consequences in more detail.

Transforming the spin operators to fermionic operators according to Eq. (12) and replacing all contractions by their mean-field values as before, one obtains

$$\langle S_{i,\alpha} S_{i+1,\beta}\rangle = -|\chi_2|^2 + 4\chi_1(\chi_0^2 - \chi_1\chi_2),$$
$$\langle S_{i,\beta} S_{i+1,\alpha}\rangle = -|\chi_1|^2 + \chi_1. \tag{24}$$

For the isotropic spin ladder, i.e., $J = J_\perp$, this gives rise to a slight dimerization: $\langle S_{i,\alpha} S_{i+1,\beta}\rangle \approx -0.22$ and $\langle S_{i,\beta} S_{i+1,\alpha}\rangle \approx -0.34$. A staggered dimerization pattern of this kind, on the other hand, emerges naturally from a Hamiltonian with staggered leg couplings such as

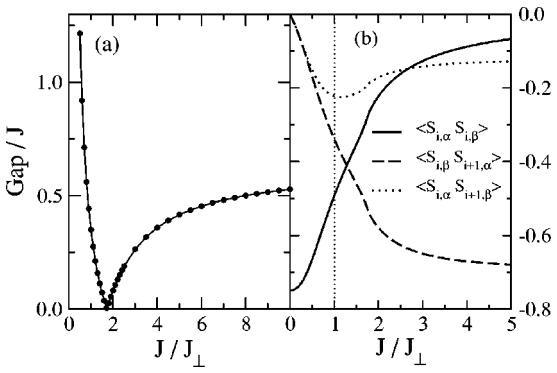

FIG. 7. Mean-field evaluation for the meander path: (a) spin gap and (b) expectation values of neighboring spin products as a function of $J/J_\perp$.

$$H = J_\perp \sum_i \mathbf{S}_{i,1}\mathbf{S}_{i,2} + \sum_i \sum_{\alpha=1,2} J[1 + \delta(-1)^{i+\alpha}]\mathbf{S}_{i,\alpha}\mathbf{S}_{i+1,\alpha}. \tag{25}$$

The properties of this Hamiltonian have been analyzed in detail.[38–40] There exists a critical line in the $(\delta, J_\perp/J)$ parameter space, where the spin gap vanishes. For $J = J_\perp$ this critical point has been located near $\delta_c \approx 0.4$.[39,40] For dimerizations δ smaller than the critical value δ_c the spin gap decreases whereas it increases again for δ larger than δ_c. Besides the reduction of the spin gap, however, the one-triplet dispersion, especially for small momenta, has been found not to depend very sensitively on the presence of a small dimerization.[40]

The analysis of Hamiltonian (25) helps to gain more insight into the underlying structure of our mean-field treatment. By introducing an artificial dimerization, the meander path recovers some of the physical properties of Hamiltonian (25). For small leg coupling the spin expectation values on both legs $\langle S_{i,\alpha} S_{i+1,\beta}\rangle$ and $\langle S_{i,\beta} S_{i+1,\alpha}\rangle$ are almost equal [see Fig. 7(b)] whereas for leg coupling $J/J_\perp > 0.4$ a noticeable dimerization develops. Consequently, the spin gap decreases more rapidly than for a two-leg ladder without dimerization [see Fig. 7(a)]. At $J/J_\perp \approx 1.7$ the dimerization reaches the critical value and the spin gap vanishes, whereas for larger leg coupling the spin gap increases again. The entire mean-field dispersions are displayed in Fig. 8. In the opposite limit,

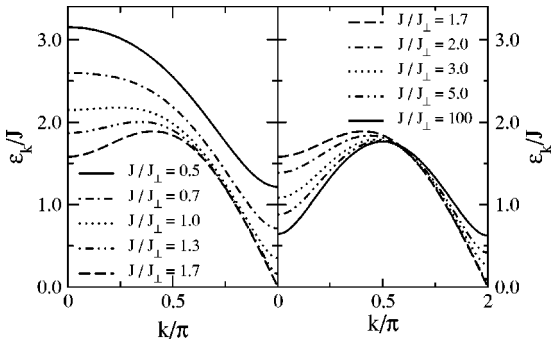

FIG. 8. Mean-field dispersion (meander path) of Jordan-Wigner fermions for different coupling ratios $J/J_\perp$.

i.e., for $J/J_\perp \to \infty$, the spin correlations along the rungs $\langle S_{i,\alpha} S_{i,\beta} \rangle$ vanish [see Fig. 7(b)]. The dimerization $\langle S_{i,\beta} S_{i+1,\alpha} \rangle - \langle S_{i,\alpha} S_{i+1,\beta} \rangle$, however, remains finite [see Fig. 7(b)], i.e., for $J/J_\perp \to \infty$ the limiting case of two decoupled dimerized spin chains is approached (see also Fig. 8).

In order to minimize the effect of the dimerization one should only consider the sum of exchange processes between sites i and $i+1$ on both legs, that is, $\langle S_{i,\alpha} S_{i+1,\beta} \rangle + \langle S_{i,\beta} S_{i+1,\alpha} \rangle$. This corresponds to contracting the two sites on the rung of the ladder to a single site, i.e., visualizing the fermionic Hamiltonian, Eq. (13), as a one-dimensional model with two fermionic species on each lattice site. This model has the full translational symmetry and therefore quantities of the two-leg ladder which are compatible with this one-dimensional model should be the least affected by dimerization.

4. The prominent role of the meander path

Certainly, the approach based on the meander path is not the only possible realization of a ''Jordan-Wigner fermionization'' for the two-leg ladder. Alternatively, the one-dimensional Jordan-Wigner transformation could also be applied along a zigzag path [see Fig. 4(b)]. Moreover, it is not necessary to adhere to a one-dimensional version of the Jordan-Wigner transformation but it is also possible to find a more symmetric formulation. These two alternative treatments are discussed in Appendix A. Nonetheless, the approach based on a meander path yields the most accurate results despite its artificially generated dimerization pattern. In the following we therefore address the puzzle, why the meander path is superior to the other (more symmetric) approaches.

The solution to this problem has to be understood from the nonequivalent treatment of spin interactions along the same leg in the different approaches. Interactions between spins succeeding along the meander path enter the Hamiltonian without further phase factors whereas interactions between the other spins transform into higher-order fermionic interaction terms and, therefore, they are captured only to lowest order in a mean-field approximation. Due to the meander-path structure only half of the leg interactions ''suffer'' from this approximation, whereas the other half of the leg interactions are treated on the same level as the rung interactions. Although this leads to an inhomogeneous treatment of the leg interactions, it is the advantage of the meander-path approach that it is possible to treat half of the leg interactions accurately. In the other Jordan-Wigner approaches, as discussed in Appendix A, all leg interactions include a phase factor which is implemented in the mean-field Hamiltonian in lowest order only. This insufficient treatment of the leg interactions is reflected in the fact that the expectation values for neighboring spin products along the legs are strongly underestimated (see Table I). The approach based on the zigzag path and the symmetric treatment yield only approximately half of the DMRG value, whereas the stronger leg bond in the meander-path approach is very close to the correct value. Strikingly, even the weaker leg bond of the meander-path approach yields a larger expectation for neighboring spin products than the other treatments.

TABLE I. Expectation values for neighboring spin products along rungs and legs for the isotropic ladder $J=J_\perp$, obtained by the Jordan-Wigner (JW) transformation based on the meander path in comparison with the other two approaches of Appendix A.

	$\langle S_{i,1} S_{i,2} \rangle$	$\langle S_{i,1/2} S_{i+1,1/2} \rangle$
DMRG	-0.46	-0.35
Meander path	-0.49	$-0.34/-0.22$
Zigzag path	-0.63	-0.16
Symmetric JW	-0.62	-0.16

The insufficient treatment of the leg interactions is visible also in the limit of two decoupled chains, i.e., for $J/J_\perp \to \infty$. Only the meander path correctly reproduces uncorrelated spins along the rungs (approaching the limit of two decoupled dimerized chains, however). In the symmetric treatment the expectation values for spin products along the legs and along the rung approach the same limit [see Fig. 18(b) in Appendix A] and for the zigzag path, the leg products even vanish [see Fig. 17(b) in Appendix A].

With these considerations we regard the Jordan-Wigner fermionization approach, based on the meander path, as the most promising choice, provided one is interested in quantities which are not too sensitive to dimerization, an aspect which will be elucidated further in the following section.

B. Dynamic correlation functions

So far we have considered only one-particle excitations of the spin ladder. The Jordan-Wigner fermionization, however, allows also the investigation of two-particle quantities. Since the approach based on the meander path proved to be the most accurate in the previous sections, we extend it to the analysis of the two-particle excitations. As a suitable example for a two-particle correlation function we will examine the magnetic contribution to the optical conductivity $\sigma(\omega)$. First, $\sigma(\omega)$ constitutes a powerful probe of the spin excitations and it has been measured on the spin ladder compound $(La,Ca)_{14}Cu_{24}O_{41}$.[18] Second, the optical conductivity can be calculated from the correlation function of neighboring spin products, a quantity with a minimum of intermediate phase factors.

Via the investigation of the optical conductivity of the spin ladder compound $(La,Ca)_{14}Cu_{24}O_{41}$ (Ref. 18) it was recently possible to verify experimentally the existence of an $S=0$ two triplet bound state in a two-leg spin ladder. This interpretation was confirmed by an evaluation based on our Jordan-Wigner treatment.[18] In a more refined analysis using the dynamical DMRG we have been able to show[20] that it is necessary to include a 4-spin cyclic exchange interaction of about $J_{cyc} \approx 0.20 J_\perp - 0.27 J_\perp$. This demonstrates that the optical conductivity is indeed an interesting quantity and is worth a more detailed discussion.

Here, for simplicity, we focus on an isotropic ladder $J=J_\perp$ without cyclic spin exchange ($J_{cyc}=0$). Although an additional cyclic spin exchange could be included straightforwardly, the number of terms in the mean-field and the RPA treatment would increase considerably. As the main pur-

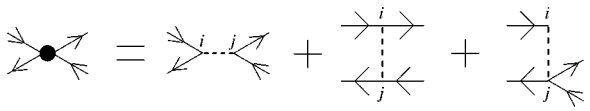

FIG. 9. Diagrammatic representation of the processes which contribute to the extended RPA treatment, in real space.

pose of the present paper is to analyze the capability of a Jordan-Wigner approach we neglect a cyclic spin-exchange term in order to keep the treatment as transparent as possible. In the following we will exhibit how the spin-flip correlation functions, which contribute to $\sigma(\omega)$, can be obtained within the Jordan-Wigner approach. Then we discuss the resulting correlation functions and focus on the $S=0$ bound state and the continuum excitations. Bound states in the singlet and triplet excitation channel were predicted by Uhrig and Schulz,[11] by Sushkov and Kotov,[12] and by Damle and Sachdev.[41] More extensive perturbative investigations were performed[13,14] and the observability of the singlet bound state was suggested by Jurecka and Brenig.[42]

For the calculation of the optical conductivity we will concentrate on an isolated Cu_2O_3 ladder. The phonon-assisted magnetic contribution to $\sigma(\omega)$ results largely from the simultaneous excitation of two neighboring spin flips and a Cu-O bond-stretching phonon:

$$\sigma(\omega)\sim -\omega\sum_{p}\sum_{p_y=0,\pi} f_p\,\mathrm{Im}\langle\langle\,\delta B_{-\mathbf{p}};\delta B_{\mathbf{p}}\rangle\rangle_{(\omega-\omega_{ph})}, \tag{26}$$

where $\mathbf{p}=(p,p_y)$ and the operators

$$\delta B^{\mathrm{leg}}_{\mathbf{p}}=\frac{1}{N}\sum_i\sum_{l=1,2} e^{i\mathbf{p}\cdot\mathbf{r}_{i,l}}(\mathbf{S}_{i,l}\mathbf{S}_{i+1,l}-\langle\mathbf{S}_{i,l}\mathbf{S}_{i+1,l}\rangle),$$

$$\delta B^{\mathrm{rung}}_{\mathbf{p}}=\frac{1}{N}\sum_i e^{i\mathbf{p}\cdot\mathbf{r}_i}(\mathbf{S}_{i,1}\mathbf{S}_{i,2}-\langle\mathbf{S}_{i,1}\mathbf{S}_{i,2}\rangle) \tag{27}$$

are the spin-flip operators for polarization of the electrical field along the legs and the rungs, respectively.

Following our previous treatment in Ref. 20, we consider phonon form factors given by

$$f_p^{\mathrm{leg}}=8\sin^4\left(\frac{p}{2}\right),\quad f_p^{\mathrm{rung}}=8\sin^2\left(\frac{p}{2}\right)+4. \tag{28}$$

Here, f_p^{leg} originates from the coupling to in-phase and out-of-phase stretching modes of O ions on the legs and it is the same form factor as for an isolated spin chain. For f_p^{rung} we take in addition to the out-of-phase stretching mode also the vibration of the O ion on the rung into account, which is responsible for the constant contribution in Eq. (28).

1. Extended RPA treatment

For the calculation of the spin-flip correlation function we apply the meander-path formulation of the Jordan-Wigner transformation (12) to the spin-flip operators $\mathbf{S}_{i,1}\mathbf{S}_{i+1,1}\pm\mathbf{S}_{i,2}\mathbf{S}_{i+1,2}$, and $\mathbf{S}_{i,1}\mathbf{S}_{i,2}$. All terms with 4- and 6-fermion operators are reduced to two-operator terms by replacing all surplus operators with their contractions (15). With this procedure the Fourier transform of the spin-flip operators becomes

$$\delta B_p^{\mathrm{rung}}=\frac{1}{\sqrt{N}}\sum_k\left(\frac{1}{2}-\chi_0\right)(\alpha_k^\dagger\beta_{p+k}+\beta_k^\dagger\alpha_{p+k}),$$

$$\delta B^{\mathrm{leg}}_{p,p_y=0}=\frac{1}{\sqrt{N}}\sum_k\{\alpha_k^\dagger\beta_{p+k}(a+be^{ik}-ce^{-i(p+k)}) +\beta_k^\dagger\alpha_{p+k}(a+be^{-i(p+k)}-ce^{ik})\},$$

$$\delta B^{\mathrm{leg}}_{p,p_y=\pi}=\frac{1}{\sqrt{N}}\sum_k\{\alpha_k^\dagger\beta_{p+k+\pi}(-a+\tilde{b}e^{ik}-ce^{-i(p+k)}) +\beta_k^\dagger\alpha_{p+k+\pi}(-a-\tilde{b}e^{-i(p+k)}+ce^{ik})\}, \tag{29}$$

with

$$a=4\chi_0\chi_1,\quad b=\tfrac{1}{2}+2\chi_0^2-4\chi_1\chi_2-\chi_1,$$

$$c=2\chi_1^2+\chi_2,\quad \tilde{b}=\tfrac{1}{2}-2\chi_0^2+4\chi_1\chi_2-\chi_1. \tag{30}$$

Inserting the spin-flip operators (29) into the optical conductivity (26) produces a sum of particle-hole propagators with different form factors. To evaluate these particle-hole propagators in RPA we prefer to use the original fermionic operators α,β because transformation to the operators $\tilde{\alpha},\tilde{\beta}$ (19) would increase the number of interaction terms considerably.

Prior to the derivation of the RPA equations, the interaction terms in the Hamiltonian have to be reduced to two-particle interactions in order to deal only with 4-particle vertices. Accordingly, all 6-operator terms, which appear in Eq. (13), are reduced to 4-operator terms by replacing all possible contractions with the corresponding bond amplitudes (15). In this way, we obtain the following reduced interaction term from Hamiltonian (13):

$$\begin{aligned}H_{\mathrm{red}}=J\frac{1}{N}\sum_{k_1,\ldots,k_4}\delta(k_1+k_2-k_3-k_4)\Big\{&\alpha_{k_1}^\dagger\beta_{k_2}^\dagger\beta_{k_3}\alpha_{k_4}\Big[\frac{J_\perp}{J}\\&+e^{i(k_2-k_3)}+(1+4\chi_2)e^{-i(k_2-k_3)}+2\chi_1(e^{i(k_1+k_2)}\\&+e^{-i(k_1+k_2)})-2\chi_0(e^{ik_1}+e^{-ik_2}+e^{ik_3}+e^{-ik_4})\Big]\\&+\alpha_{k_1}^\dagger\alpha_{k_2}^\dagger\beta_{k_3}\beta_{k_4}2\chi_1e^{i(k_2-k_3)}\\&+\beta_{k_1}^\dagger\beta_{k_2}^\dagger\alpha_{k_3}\alpha_{k_4}2\chi_1e^{i(k_1-k_4)}\Big\}.\end{aligned} \tag{31}$$

A set of RPA equations for the particle-hole propagators, which are listed in Appendix B, can be obtained by consideration of all possible vertex configurations of the interaction Hamiltonian (31). In real space these vertices correspond not only to a summation of bubble diagrams, but also include ladder diagrams and other nonlocal terms as indicated in Fig. 9. For this reason we use the term *extended* RPA treatment.

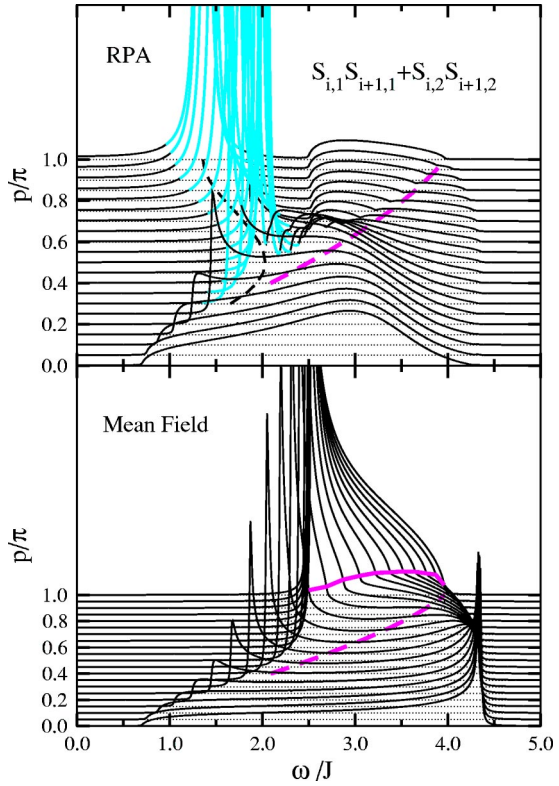

FIG. 10. RPA and mean-field evaluation of the momentum resolved correlation function $\langle\langle \delta B^{\mathrm{leg}}_{-p,p_y=0}; \delta B^{\mathrm{leg}}_{p,p_y=0}\rangle\rangle$, where a broadening of $\delta=0.01J$ has been used. The gray lines (upper panel) designate the $S=0$ bound state. The dashed dark gray line is a projection of the dark gray line in the lower panel, which links the points of sharp increase in the middle of the continuum. This is a precursor of the upper edge of the 2-spinon continuum in single chains (Refs. 14 and 43). In RPA a dip structure remains at the same position in the continuum.

2. Spin-flip correlation functions

In this section the correlation functions for spin flips along the legs $\delta B^{\mathrm{leg}}_{p,p_y=0}$, $\delta B^{\mathrm{leg}}_{p,p_y=\pi}$ and for spin flips along the rungs $\delta B^{\mathrm{rung}}_{p}$ for an isotropic ladder $J=J_\perp$, using the RPA treatment of the preceding section, will be discussed. The results are presented in Figs. 10, 12, and 13. For comparison the mean-field evaluation of each of the correlation functions is displayed in the lower panels.

In the mean-field evaluation of $\langle\langle \delta B^{\mathrm{leg}}_{-p,p_y=0}; \delta B^{\mathrm{leg}}_{p,p_y=0}\rangle\rangle$ (lower panel of Fig. 10) one observes Van Hove singularities at the upper edge of the continuum for small momenta and at the lower edge of the continuum for large momenta. With the RPA treatment the Van Hove singularities at the continuum edges disappear. For small momenta the maximum of the continuum is shifted from the upper edge downwards to about $\omega\approx 3J$. At large momenta we observe the formation of the $S=0$ bound state. The bound state emerges from the continuum at $k\approx 0.3\pi$, it passes through a maximum at $k\approx\pi/2$ and a minimum at $k=\pi$. In Fig. 11 the dispersion of the bound state is compared with the DMRG calculation for an $N=80$ site ladder.[20] We find good agreement between both methods, only the energy of the RPA dispersion is slightly too low. This indicates that the interaction strength is somewhat overestimated in RPA.

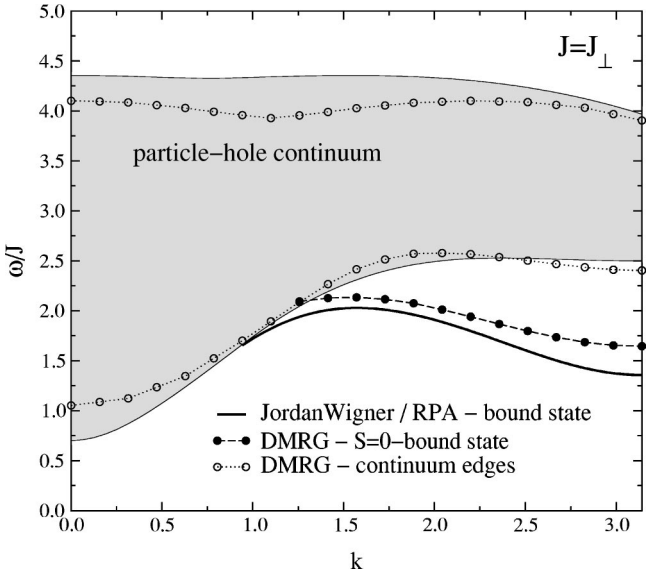

FIG. 11. Particle-hole continuum of the Jordan-Wigner fermions and $S=0$ bound state (thick solid line) in comparison with the two-triplet continuum (open symbols) and $S=0$ bound state (filled symbols) obtained by DMRG for a ladder with $N=80$ sites (Ref. 20).

In the mean-field evaluation of the out-of-phase component of the correlation function for spin flips along the legs $\langle\langle \delta B^{\mathrm{leg}}_{-p,p_y=\pi}; \delta B^{\mathrm{leg}}_{p,p_y=\pi}\rangle\rangle$ (lower panel in Fig. 12) the Van Hove singularities at the continuum edges are suppressed. The overall momentum dependence on p appears to be reversed when the out-of-phase component in Fig. 12 (upper panel) is compared to the in-phase component in Fig. 10 (upper panel). This is caused by the checkerboard sublattice structure of the meander path, which shifts the momentum of the particle-hole propagator $\delta B^{\mathrm{leg}}_{p,p_y=\pi}$ by π in relation (29). The inversion of the momentum dependence is especially noticeable for the bound state. However, the out-of-phase component should not contain the bound state but only contribute to the continuum excitations, an issue that we have addressed previously in Ref. 20. The argument is based on the observation that the out-of-phase component originates from the excitation of three different rung triplets,[20] when it is expressed in terms of rung-triplet operators.[9,10] The $S=0$ bound state, on the other hand, arises from scattering processes of two equal triplets and therefore cannot be present in the out-of-phase component. The spurious appearance of the bound state in the out-of-phase component demonstrates the sensitivity of the out-of-phase mode to an artificial dimerization. This sensitivity is due to the fact that the out-of-phase mode is calculated as the correlation function of the difference of neighboring spin products $\mathbf{S}_{i,1}\mathbf{S}_{i+1,1}-\mathbf{S}_{i,2}\mathbf{S}_{i+1,2}$, i.e., a term whose expectation value is just the dimerization. On the other hand this also explains, why the in-phase mode is much less sensitive to dimerization as it corresponds to the sum of neighboring spin products $\mathbf{S}_{i,1}\mathbf{S}_{i+1,1}+\mathbf{S}_{i,2}\mathbf{S}_{i+1,2}$.

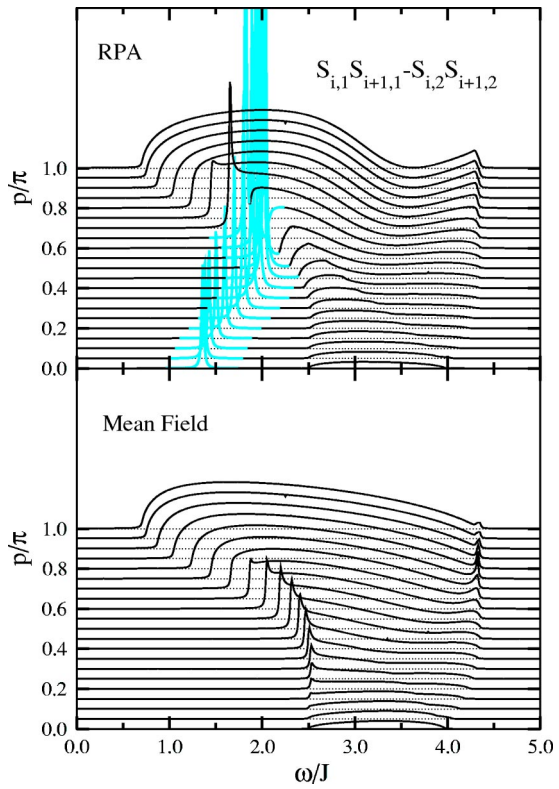

FIG. 12. RPA and mean-field evaluation of the correlation function $\langle\langle \delta B^{\mathrm{leg}}_{-p,p_y=\pi}; \delta B^{\mathrm{leg}}_{p,p_y=\pi}\rangle\rangle$, where a broadening of $\delta=0.01J$ has been used. The gray lines indicate the $S=0$ bound state.

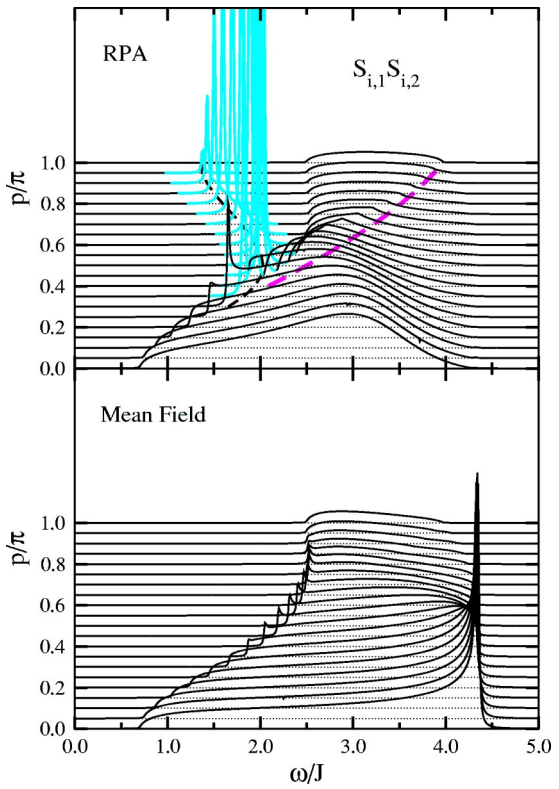

FIG. 13. RPA and mean-field evaluation of the correlation function $\langle\langle \delta B^{\mathrm{rung}}_{-p}; \delta B^{\mathrm{rung}}_{p}\rangle\rangle$, where a broadening of $\delta=0.01J$ has been used. The gray lines indicate the $S=0$ bound state. The dashed dark gray line in the upper panel is the same as in Fig. 10.

In Fig. 13 the RPA and mean-field evaluation for the correlation function of spin flips along the rungs $\langle\langle \delta B^{\mathrm{rung}}_{-p}; \delta B^{\mathrm{rung}}_{p}\rangle\rangle$ are shown in the upper and lower panels, respectively. For $p=0$ it is identical to the $p=0$ component of the in-phase correlation function for spin flips along the legs $\langle\langle \delta B^{\mathrm{leg}}_{-p,p_y=0}; \delta B^{\mathrm{leg}}_{p,p_y=0}\rangle\rangle$ and both correspond to the correlation function for the Raman response.[44,45] For larger momenta, the spectral weight of the rung correlation is much smaller than the in-phase component of the leg correlations and at $p=\pi$ the weight of the $S=0$ bound state vanishes according to a selection rule,[18] which originates in the reflection symmetry of a singlet state of two rung triplets about any rung axis. Since the operator for spin flips along the rungs $\delta B^{\mathrm{rung}}_{p}$ is odd under this symmetry at $p=\pi$ the weight of the singlet bound state for its excitation with momentum $p=\pi$ is zero.

3. Optical conductivity

Once the momentum dependent spin-flip correlation functions, shown in Figs. 10, 12, and 13, are known, the optical conductivity $\sigma(\omega)$ in Eq. (26) can easily be obtained by integration. In Fig. 14 the in-phase $p_y=0$ and the out-of-phase $p_y=\pi$ contribution to $\sigma(\omega)$ for polarization along the legs are displayed in the upper two panels. The optical conductivity for polarization along the rungs is shown in the lower panel of Fig. 14. In all panels the corresponding DMRG spectrum, obtained with the correction-vector method,[27] has been added in order to facilitate a judgment about the accuracy of our Jordan-Wigner approach.

For polarization parallel to the legs and $p_y=0$ (top panel of Fig. 14) two dominant peaks appear at $\omega_1\approx 1.4J$ and $\omega_2\approx 2.0J$. They are caused by Van Hove singularities arising from the dispersion of the $S=0$ bound state[18] at $p=\pi$ and $p\approx\pi/2$. The upper peak at ω_2 is suppressed by the inclusion of the relevant form factor $\sin^4(p/2)$. For the $p_y=0$ component we find reasonable agreement with the corresponding DMRG spectrum. The frequency of the $S=0$ bound state is somewhat too low in the Jordan-Wigner approach because the RPA treatment overestimates the interaction strength as discussed in Sec. III B 2. The continuum contribution, on the other hand, is slightly underestimated. To some extent this is due to the fact that, so far, we have considered only the creation of two fermions at the external current vertex: we approximated the spin-flip operators in Eq. (29) by a particle-hole creation operator. Without this approximation the correlation functions $\langle\langle \delta B^{\mathrm{leg}}_{-p,p_y=0,-\pi}; \delta B^{\mathrm{leg}}_{p,p_y=0,\pi}\rangle\rangle$ would contain the excitation of 4- and 6-fermions as well, which would increase the amount of high-energy excitations. The weight of these higher-order excitations will be estimated in the following section.

With respect to the out-of-phase component (middle panel of Fig. 14), however, there is only poor agreement with the DMRG spectrum. To some extent this is due to the importance of higher-order processes which make up about 50% of the weight of the out-of-phase mode as discussed in the fol-

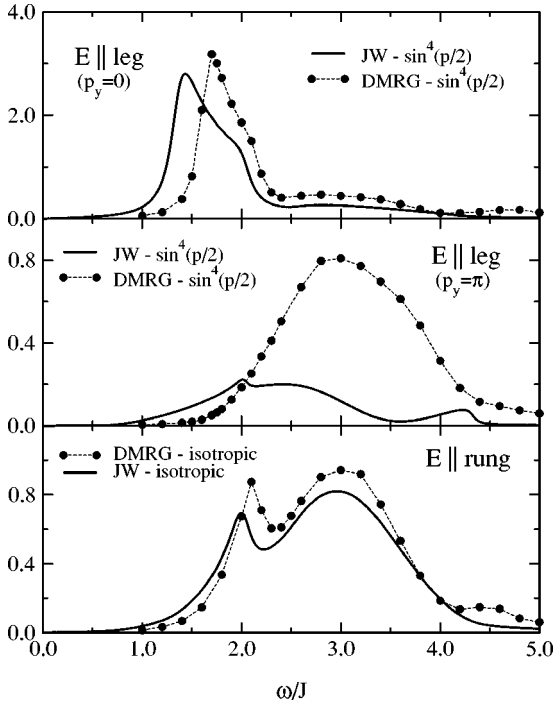

FIG. 14. Momentum integrated spin-flip correlation functions, which contribute to $\sigma(\omega)$ for polarization along the legs (top and middle panel) and for polarization along the rungs (bottom panel). In order to visualize the resulting contribution to $\sigma(\omega)$ in Eq. (26) each correlation function has been multiplied with the frequency ω and for each of them the momentum integration is shown without a prefactor (dashed lines) and with a prefactor of $\sin^4(p_x/2)$, i.e., $\sin^2(p_x/2)$ (solid lines). In each panel one DMRG spectrum (symbols) has been added for comparison.

lowing section. Furthermore the stronger sensitivity of the out-of-phase mode to dimerization is adverse, as explained in the preceding section.

For polarization parallel to the rungs (bottom panel of Fig. 14) only the upper bound state at ω_2 is present in the momentum integrated spectrum because the $S=0$ bound state is suppressed at $p=\pi$ in accord with a selection rule,[18] see also Fig. 13. For the rung polarization we find very good agreement with the DMRG result. Rung correlations are obviously treated quite accurately in our meander-path representation. There are no phase factors in the product of two spin operators on the same rung because they are neighboring along the meander path. Therefore the only 4-fermion process results from an Ising-like term.

4. Higher-order contributions

The contribution of 4 and 6 fermions to the spin-flip correlation functions in leg polarization can be obtained analogous to the 2-fermion contribution. In the spin-flip operator $\delta B_p^{\mathrm{leg}}$, Eq. (27), the spin operators are replaced by fermionic operators. Terms with 6 operators are designated as the 6-fermion part. Terms with 4 and 6 operators contribute to the 4-fermion part, when all surplus operators are replaced by their contractions, analogous to Eq. (29). With this scheme one obtains for the 4- and 6-fermion part of the spin-flip operator

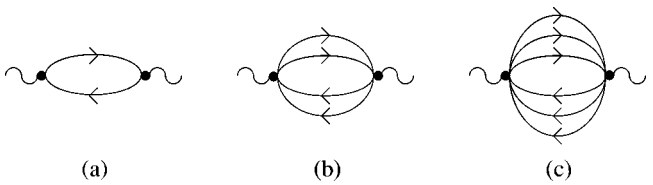

FIG. 15. Mean-field weights for the spin-flip correlation. They correspond to the evaluation of one, two, and three noninteracting particle-hole lines for the excitation of 2-, 4-, and 6-fermions displayed in (a), (b), and (c), respectively.

$$\begin{aligned}\delta B^{4,\mathrm{leg}}_{p,p_y=0} = \frac{1}{N^{3/2}} \sum_{k_1,\ldots,k_4} 2\,\delta(p+k_1+k_2-k_3-k_4)\\ \times\Big\{ \alpha^\dagger_{k_1}\beta^\dagger_{k_2}\beta_{k_3}\alpha_{k_4}\Big[\chi_1(e^{i(k_1+k_2)}+e^{-i(k_3+k_4)})\\ -\chi_0(e^{ik_1}+e^{-ik_4}+e^{-i(p+k_2)}+e^{-i(p-k_3)})\\ +\frac{1}{2}(e^{i(k_2-k_3)}+e^{i(k_1-k_4)})+2\chi_2 e^{i(k_1-k_4)}\Big]\\ +\alpha^\dagger_{k_1}\alpha^\dagger_{k_2}\beta_{k_3}\beta_{k_4}\chi_1 e^{i(k_2-k_3)}\\ +\beta^\dagger_{k_1}\beta^\dagger_{k_2}\alpha_{k_3}\alpha_{k_4}\chi_1 e^{i(k_1-k_4)}\Big\},\end{aligned}$$

$$\begin{aligned}\delta B^{6,\mathrm{leg}}_{p,p_y=0} = \frac{1}{N^{5/2}} \sum_{k_1,\ldots,k_6} 2\,\delta(p+k_1+k_2+k_3-k_4-k_5-k_6)\\ \times\{\alpha^\dagger_{k_1}\alpha^\dagger_{k_2}\beta^\dagger_{k_3}\beta_{k_4}\beta_{k_5}\alpha_{k_6}e^{i(k_2-k_4-k_6)}\\ +\alpha^\dagger_{k_1}\beta^\dagger_{k_2}\beta^\dagger_{k_3}\beta_{k_4}\alpha_{k_5}\alpha_{k_6}e^{i(k_1+k_2-k_6)}\}\end{aligned} \tag{32}$$

for the in-phase component of the leg polarization. The out-of-phase component is very similar, except that the momentum p has to be replaced with $(p+\pi)$ and, in the term $\frac{1}{2}(e^{i(k_2-k_3)}+e^{i(k_1-k_4)})\alpha^\dagger_{k_1}\beta^\dagger_{k_2}\beta_{k_3}\alpha_{k_4}$ of the 4-fermion component, the parentheses have to be replaced with $(e^{i(k_2-k_3)}-e^{i(k_1-k_4)})$.

In order to estimate the contribution of processes involving the excitation of a different number of fermions, we compare the weights

$$W^n_{p_y} = -\int_0^\infty d\omega \frac{1}{N}\sum_p f_p \langle\langle \delta B^n_{-p,p_y}; \delta B^n_{p,p_y}\rangle\rangle, \tag{33}$$

which are obtained by integrating the $n=2$, 4, and 6 fermion part of the leg-correlation functions over frequency ω and momentum p using form factors $f_p=1$ and $f_p=\sin^4(p/2)$. To keep this evaluation as simple as possible the correlation functions are evaluated in mean-field theory, i.e., they are replaced by noninteracting particle-hole lines as indicated in Fig. 15. The frequency integrals in Eq. (33) can be eliminated using

TABLE II. Mean-field weights of the 2-, 4-, and 6-fermion contributions to the in-phase ($p_y=0$) and the out-of-phase ($p_y=\pi$) component assuming noninteracting particle-hole lines. For the 2-fermion contribution the weight of the RPA evaluation is given in parentheses.

	$p_y=0$ $f_p=1$	$p_y=0$ $f_p=\sin^4(p/2)$	$p_y=\pi$ $f_p=1$	$p_y=\pi$ $f_p=\sin^4(p/2)$
$n=2$	1.88	0.95	0.25	0.17
	(2.56)	(1.47)	(0.25)	(0.17)
$n=4$	0.59	0.17	0.45	0.17
$n=6$	0.01	0.01	0.01	0.01

$$\pi\prod_j a_j = -\mathrm{Im}\int_0^\infty d\omega\, e^{i\omega 0^+}\prod_j \frac{1}{2\pi i}\int_{-\infty}^{\infty} d\Omega_j\,\delta\Big(\omega-\sum_j \Omega_j\Big) \times\Big(\frac{a_j}{\Omega_j-\epsilon_j+i0^+}+\frac{b_j}{\Omega_j+\epsilon_j-i0^+}\Big), \tag{34}$$

where $a_j/(\Omega_j\mp\epsilon_j\pm i0^+)$ are expressions for retarded and advanced Green's functions. The remaining momentum integrals can be easily evaluated numerically.

The resulting weights of the 2-, 4-, and 6-fermion processes are displayed in Table II. The 4- and 6-fermion processes make up only 24% [15%] of the in-phase part of the spin-flip correlation function when a form factor of $f_p=1$ [$f_p=\sin^4(p/2)$] is used. On the other hand, they generate a major contribution to the out-of-phase component, i.e., 65% [50%]. Note that these values refer only to noninteracting particle-hole propagators and may be changed when the evaluation is improved. For example, the weight of the 2-fermion contribution to the in-phase component is enhanced when the particle-hole propagator is evaluated in RPA. In Table II these RPA weights are added in parentheses.

Since the 4- and 6-fermion processes contribute only to the continuum excitations, they will increase the high-energy weight and therefore improve the consistency with the DMRG results for polarization along the legs in Fig. 14. Presumably, however, the consideration of a direct excitation of 4- and 6-fermion processes will not suffice to obtain full agreement with the DMRG spectra. It might also be necessary to include higher-order vertex corrections. They may shift some weight from the bound state to the continuum excitations, because the RPA overestimates the interaction strength as discussed in Sec. III B 2. They may also help to reduce the artificially introduced dimerization by the meander path which has been discussed in Sec. III A 3.

IV. CONCLUSIONS

In this paper we presented an approach to obtain dynamic correlation functions in low-dimensional quantum spin systems. It is based on a fermionization of spin operators through a Jordan-Wigner transformation and it treats the fermionic interactions in RPA. We demonstrated that the application of standard perturbation theory to the new fermionic operators is appropriate even in the high-energy range. We considered the 1D spin-1/2 chains as an appropriate case study and tested the validity of the approach through the evaluation of a specific dynamical spin-flip correlation function. This correlation function corresponds to the phonon-assisted magnetic contribution to the optical conductivity, and we found good agreement with the experimental spectrum of Sr_2CuO_3.

In order to extend this approach to two-leg $S=\frac{1}{2}$ ladders we have analyzed different possibilities to apply the Jordan-Wigner transformation to a two-leg spin ladder. In contrast to the 1D spin chain, however, operator phase factors emerge even in the Hamiltonian. Expanding these phase factors creates new interaction terms, which can be treated within standard perturbation theory. We elaborated that it is essential to include fluctuations which originate from the phase factors—rather than treating the phases as c numbers. Applying the Jordan-Wigner transformation along a meander path through the ladder allows us to treat half of the leg interactions on the same level as the rung interactions. This advantage outweighs the artifact of introducing a slight dimerization of the spin ladder: the resulting one-triplet dispersion agrees well with the DMRG result, much better than other more symmetric realizations of the Jordan-Wigner transformation.

Based on the meander-path approach we have developed an extended RPA scheme for calculating the dynamical two-spin correlation function, the basic ingredient for the optical conductivity. In order to test the accuracy of our approach we have compared our results with spectra obtained from a dynamical DMRG. For polarization along the rungs we find very good agreement with the DMRG spectra. Spin-flip processes on the rungs are represented quite reliably in our approach, because two spins on the same rung are also neighboring along the meander path. Therefore no phase factor is present in the corresponding spin-flip operator. For spin-flip processes along the legs, however, the phase factor generates the excitation of 4 and 6 fermions in addition to the 2-fermion processes. With respect to the $S=0$ bound state convincing results already emerge from the evaluation of the 2-fermion contribution. The weight of the high-energy continuum, however, is underestimated. To some extent this can be compensated by the consideration of 4- and 6-fermion excitations.

In this paper we have focused on two-leg spin-1/2 ladders. It would certainly be interesting to extend this treatment to ladders with more than two legs. With respect to odd-leg ladders it is promising that the fermionic approach naturally reproduces the gapless excitation spectrum of odd-leg ladders. Without magnetic field the fermionic system is at half filling and consequently, for an odd number of fermionic bands, one band is half filled which accounts for the absence of a spin gap.

ACKNOWLEDGMENTS

We would like to thank M. Grüninger and Q. Yuan for stimulating discussions. This project was supported by the DFG (SFB 484) and by the BMBF (13N6918 A).

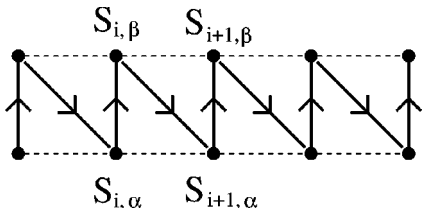

FIG. 16. Sublattice structure for the zigzag path.

APPENDIX A: FURTHER APPROACHES TO JORDAN-WIGNER TRANSFORMATIONS

This appendix addresses other possible Jordan-Wigner treatments of the two-leg spin ladder and their resulting mean-field Hamiltonians. Besides the meander path, which our Jordan-Wigner approach is based on, the one-dimensional Jordan-Wigner transformation could also be applied along a zigzag path. This alternative choice is discussed in Sec. A 1. Moreover, it is not necessary to stick to a one-dimensional version of the Jordan-Wigner transformation but it is also possible to find a more symmetric formulation as discussed in Sec. A 2.

1. Zigzag path

The sublattice structure underlying the zigzag path is very simple: each leg corresponds to one sublattice, as indicated in Fig. 16. Applying the one-dimensional Jordan-Wigner transformation, Eq. (12), along the zigzag path with the sublattice structure of Fig. 16 generates the following Hamiltonian:

$$H = J_\perp \sum_i \left\{ \frac{1}{2}(\alpha_i^\dagger \beta_i + \beta_i^\dagger \alpha_i) + \left(\alpha_i^\dagger \alpha_i - \frac{1}{2} \right) \left(\beta_i^\dagger \beta_i - \frac{1}{2} \right) \right\}$$
$$+ J \sum_i \left\{ \frac{1}{2} [\alpha_i^\dagger \alpha_{i+1} (1 - 2\beta_i^\dagger \beta_i) + \beta_i^\dagger \beta_{i+1}$$
$$\times (1 - 2\alpha_{i+1}^\dagger \alpha_{i+1}) + \text{H.c.}] + \left(\alpha_i^\dagger \alpha_i - \frac{1}{2} \right)$$
$$\times \left(\beta_{i+1}^\dagger \beta_{i+1} - \frac{1}{2} \right) + \left(\alpha_{i+1}^\dagger \alpha_{i+1} - \frac{1}{2} \right) \left(\beta_i^\dagger \beta_i - \frac{1}{2} \right) \right\}. \tag{A1}$$

Here the expansion of the phase factor yields only 4-operator terms. Taking into account all nearest- and next-nearest-neighbor bond amplitudes

$$\chi_0 = \langle \beta_i^\dagger \alpha_i \rangle, \quad \chi_1 = \langle \beta_i^\dagger \alpha_{i+1} \rangle, \quad \chi_2 = \langle \alpha_i^\dagger \beta_{i+1} \rangle,$$
$$\chi_3 = \langle \alpha_i^\dagger \alpha_{i+1} \rangle, \quad \chi_4 = \langle \beta_i^\dagger \beta_{i+1} \rangle, \tag{A2}$$

the following mean-field Hamiltonian is obtained:

$$H_{\text{MF}} = \sum_k \{ \gamma_{0,k} \alpha_k^\dagger \beta_k + \gamma_{0,k}^* \beta_k^\dagger \alpha_k + \gamma_{\alpha,k} \alpha_k^\dagger \alpha_k + \gamma_{\beta,k} \beta_k^\dagger \beta_k \}, \tag{A3}$$

with

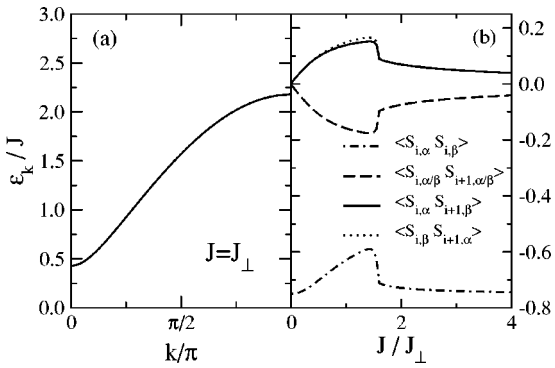

FIG. 17. Mean-field treatment based on the zigzag path: (a) dispersion for $J = J_\perp$ and (b) expectation values for neighboring spin products as a function of $J/J_\perp$.

$$\gamma_{0,k} = J_\perp (\tfrac{1}{2} - \chi_0) + 2J(\chi_0 e^{ik} + \chi_1),$$
$$\gamma_{\alpha,k} = -2J\,\text{Re}(\chi_4 + \chi_3 e^{ik}), \quad \gamma_{\beta,k} = -2J\,\text{Re}(\chi_3 + \chi_4 e^{ik}). \tag{A4}$$

Diagonalization of the mean-field Hamiltonian results in

$$H_{MF} = \sum_k (\epsilon_{\alpha,k} \tilde{\alpha}_k^\dagger \tilde{\alpha}_k + \epsilon_{\beta,k} \tilde{\beta}_k^\dagger \tilde{\beta}_k), \tag{A5}$$

with

$$\epsilon_{\alpha/\beta,k} = \frac{\gamma_{\alpha,k} + \gamma_{\beta,k}}{2} \pm \sqrt{\left(\frac{\gamma_{\alpha,k} - \gamma_{\beta,k}}{2} \right)^2 + |\gamma_0|^2}. \tag{A6}$$

For the isotropic ladder $J_\perp = J$ the mean-field evaluation yields $\chi_0 = -0.437$, $\chi_1 = 0.180$, $\chi_2 = -0.136$, $\chi_3 = \chi_4 = 0$ and therefore $\gamma_{\alpha,k} = \gamma_{\beta,k} = 0$. The expectation values of neighboring spin products are displayed in Fig. 17(b) as a function of $J/J_\perp$. For the zigzag path there is no dimerization with respect to the spin products along the legs. However, a slight difference in the expectation values for the products of spin operators situated along the diagonals appears for intermediate values of $J/J_\perp$, which reflects the type of symmetry reduction due to the zigzag path. In the limit of strong rung coupling $J/J_\perp = 0$ the correct ground state is recovered, which consists of singlets along the rungs. For $J/J_\perp \to \infty$, however, the expectation values for spin products on the rungs spuriously approach the same limit as for $J/J_\perp = 0$.

Also the mean-field dispersion, which is displayed in Fig. 17(a) for $J = J_\perp$, shows only poor agreement with the expected one-triplet dispersion. This discrepancy already arises in the strong-coupling limit since one obtains

$$\gamma_{0,k} = J_\perp - J(\cos k + i \sin k), \quad \gamma_{\alpha,k} = \gamma_{\beta,k} = 0 \tag{A7}$$

by inserting the zeroth-order bond amplitudes $\chi_0 = -\frac{1}{2}$, $\chi_1 = \chi_2 = \chi_3 = \chi_4 = 0$. For the dispersion this produces to first order in $J/J_\perp$,

$$\epsilon_k = |\gamma_{0,k}| = J_\perp \sqrt{1 - 2\frac{J}{J_\perp} \cos k + \left(\frac{J}{J_\perp} \right)^2} \approx J_\perp - J \cos k, \tag{A8}$$

which obviously differs from the correct strong-coupling limit (23).

2. General treatment of the two-leg ladder

It is not necessary to apply the Jordan-Wigner transformation along a one-dimensional path through the two-leg ladder. More generally the Jordan-Wigner transformation can be written as

$$S_i^\dagger = c_i^\dagger e^{i\pi\phi_i} \quad \text{with} \quad \phi_i = \sum_{j\neq i} \varphi_{ij} c_j^\dagger c_j . \tag{A9}$$

In order to fulfill the correct commutation relations for the spin operators the phase factors φ_{ij} have to obey

$$\varphi_{ij} = \varphi_{ji} \pm 1 . \tag{A10}$$

This relation is automatically fulfilled by arranging the spins in a one-dimensional sequence as $\varphi_{i,i+1}=1$ and $\varphi_{i+1,i}=0$. The phase factor, however, can also be distributed among the spins in a more symmetric way by choosing, e.g.,

$$S_{i,\alpha}^+ = \alpha_i^\dagger \exp\left[i\pi \sum_{j<i} (\alpha_j^\dagger \alpha_j + \beta_j^\dagger \beta_j) \right] e^{i(\pi/2)\beta_i^\dagger \beta_i},$$

$$S_{i,\beta}^+ = \beta_i^\dagger \exp\left[i\pi \sum_{j<i} (\alpha_j^\dagger \alpha_j + \beta_j^\dagger \beta_j) \right] e^{-i(\pi/2)\alpha_i^\dagger \alpha_i}. \tag{A11}$$

Now the sublattice of the $\mathbf{S}_{i,\alpha}$ and $\mathbf{S}_{i,\beta}$ spins can be arranged in a checkerboard-type structure such as for the meander path (see Fig. 5) or with respect to the legs such as for the zigzag path (see Fig. 16).

Here, we will only discuss the checkerboard-type sublattice. Using the above version of the Jordan-Wigner transformation (A11) and expanding the phase factor the Hamiltonian for the checkerboard-type sublattice transforms to

$$\begin{aligned} H = {} & J_\perp \sum_i \left\{ \frac{1}{2}(\alpha_i^\dagger \beta_i + \beta_i^\dagger \alpha_i) + \left(\alpha_i^\dagger \alpha_i - \frac{1}{2} \right) \left(\beta_i^\dagger \beta_i - \frac{1}{2} \right) \right\} \\ & + J \sum_i \left\{ \frac{1}{2} [\alpha_i^\dagger \beta_{i+1} (1-(i+1)\beta_i^\dagger \beta_i)(1+(i-1) \right. \\ & \times \alpha_{i+1}^\dagger \alpha_{i+1}) + \beta_i^\dagger \alpha_{i+1} (1+(i-1)\alpha_i^\dagger \alpha_i)(1-(i+1) \\ & \left. \times \beta_{i+1}^\dagger \beta_{i+1}) + \text{H.c.}] + \left(\alpha_i^\dagger \alpha_i - \frac{1}{2} \right) \left(\beta_{i+1}^\dagger \beta_{i+1} - \frac{1}{2} \right) \right. \\ & \left. + \left(\alpha_{i+1}^\dagger \alpha_{i+1} - \frac{1}{2} \right) \left(\beta_i^\dagger \beta_i - \frac{1}{2} \right) \right\}. \end{aligned} \tag{A12}$$

Considering all nearest- and next-nearest-neighbor bond amplitudes as in Eq. (A2) one obtains a mean-field Hamiltonian with the same structure as for the zigzag path (A3). Therefore also the mean-field dispersion is of form (A6) with

$$\begin{aligned} \gamma_{0,k} = {} & J_\perp (\tfrac{1}{2} - \chi_0) + J(2\chi_0^* \chi_1 + 2\chi_0^* \chi_2^* + \text{Im}\chi_3 - \text{Im}\chi_4) \\ & + Je^{ik}(\tfrac{1}{4} - |\chi_2|^2 + \chi_0^2 - \chi_1\chi_2 - \chi_1\chi_2^* - \chi_1 + \chi_3\chi_4) \\ & + Je^{-ik}(\tfrac{1}{4} - |\chi_1|^2 + \chi_0^2 - \chi_1^*\chi_2^* - \chi_1\chi_2^* - \chi_2^* + \chi_3^*\chi_4^*), \\ \gamma_{\alpha,k} = {} & -J[\text{Im}(\chi_1+\chi_2) + 2\text{Re}\chi_0(\sin k + 2\text{Re}\chi_4) \\ & - 2\text{Re}(\chi_1\chi_4^* + \chi_2\chi_4^*)e^{ik}], \\ \gamma_{\beta,k} = {} & J[\text{Im}(\chi_1+\chi_2) + 2\text{Re}\chi_0(\sin k - 2\text{Re}\chi_3) \\ & + 2\text{Re}(\chi_1\chi_3^* + \chi_2\chi_3^*)e^{ik}]. \end{aligned} \tag{A13}$$

For $J=J_\perp$ the bond amplitudes yield $\chi_0=-0.431$, $\chi_1=\chi_2=-0.028$, $\chi_3=-\chi_4=0.162i$ and the resulting mean-field dispersion for $J=J_\perp$ is displayed in Fig. 18(a). Although there is no artificial dimerization in this symmetric treatment, the resulting mean-field dispersion [solid line in Fig. 18(a)] deviates more from the DMRG result than the dispersion obtained by the meander-path treatment [dashed line in Fig. 18(a)]. In the limit of large leg coupling $J/J_\perp$ the expectation value for spin products along the rungs approaches the same value as the expectation value for products of neighboring spins along the legs. This is certainly not the correct limit as rung spins should be uncorrelated for $J/J_\perp \to \infty$.

APPENDIX B: RPA EQUATIONS

The RPA equations for the particle-hole propagators of the spinless Jordan-Wigner fermions can be obtained by considering all possible vertex configurations of the RPA Hamiltonian (31). The explicit form for the renormalized particle-hole propagators is

$$\begin{aligned} B^{\mu,\nu}_{\gamma^\dagger\rho,\delta\sigma^\dagger} = {} & \tilde{b}^{\mu,\nu}_{\gamma^\dagger\rho,\delta\sigma^\dagger} + \sum_{\lambda=0}^{2} \{ b^{\mu,3\lambda}_{\gamma^\dagger\alpha,\delta\alpha^\dagger} B^{\lambda,\nu}_{\beta^\dagger\rho,\beta\sigma^\dagger} \\ & + b^{\mu,1\lambda}_{\gamma^\dagger\alpha,\delta\beta^\dagger} B^{\lambda,\nu}_{\alpha^\dagger\rho,\beta\sigma^\dagger} + b^{\mu,6\lambda}_{\gamma^\dagger\alpha,\delta\beta^\dagger} B^{\lambda,\nu}_{\beta^\dagger\rho,\alpha\sigma^\dagger} \\ & + b^{\mu,4\lambda}_{\gamma^\dagger\beta,\delta\alpha^\dagger} B^{\lambda,\nu}_{\beta^\dagger\rho,\alpha\sigma^\dagger} + b^{\mu,5\lambda}_{\gamma^\dagger\beta,\delta\alpha^\dagger} B^{\lambda,\nu}_{\alpha^\dagger\rho,\beta\sigma^\dagger} \\ & + b^{\mu,2\lambda}_{\gamma^\dagger\beta,\delta\beta^\dagger} B^{\lambda,\nu}_{\alpha^\dagger\rho,\alpha\sigma^\dagger} \}. \end{aligned} \tag{B1}$$

For simplicity the momentum and frequency indices p and ω have been omitted. The noninteracting particle-hole propagators $\tilde{b}$ and b, including the appropriate form factors from the internal interaction vertices, are defined as

$$\tilde{b}^{\mu,\nu}_{\gamma^\dagger\rho,\delta\sigma^\dagger} = \frac{1}{N} \sum_k f_k^\mu f_k^\nu b^0_{\gamma^\dagger\rho,\delta\sigma^\dagger}(p,k,\omega),$$

$$b^{\mu,s\lambda}_{\gamma^\dagger\rho,\delta\sigma^\dagger} = \frac{1}{N} \sum_k f_k^\mu g^{(s,\lambda)}(p,k) b^0_{\gamma^\dagger\rho,\delta\sigma^\dagger}(p,k,\omega), \tag{B2}$$

with form factors

$$f_k^0 = 1, \quad f_k^1 = e^{ik}, \quad f_k^2 = e^{-ik}, \tag{B3}$$

and

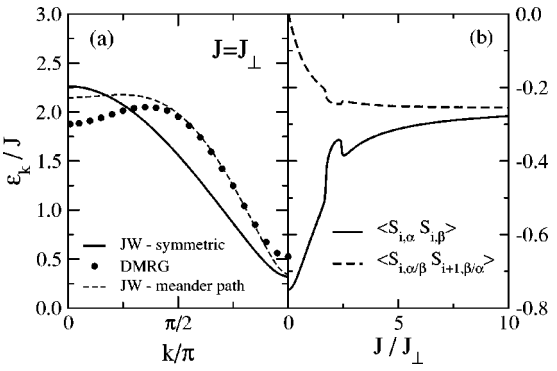

FIG. 18. Mean-field treatment of Hamiltonian (A12): (a) dispersion for $J=J_\perp$ (solid line). For comparison the dispersion obtained by the meander-path treatment (dashed line) and the DMRG dispersion are added. (b) Expectation values for neighboring spin products as a function of $J/J_\perp$.

$$g^{(1,0)}(p,k)=-J_\perp f_k^0+2J\chi_0(1+e^{-ip})f_k^2,$$

$$g^{(1,1)}(p,k)=J[2\chi_0(1+e^{ip})f_k^0-2\chi_1 e^{ip}f_k^1-(1+4\chi_2)f_k^2],$$

$$g^{(1,2)}(p,k)=-J(f_k^1+2\chi_1 e^{-ip}f_k^2),$$

$$g^{(2,0)}(p,k)=[J_\perp+J\{e^{-ip}+(1+4\chi_2)e^{ip}\}]f_k^0-2J\chi_0 e^{ip}f_k^1-2J\chi_0 f_k^2,$$

$$g^{(2,1)}(p,k)=2J(-\chi_0 e^{ip}f_k^0+\chi_1 e^{ip}f_k^1),$$

$$g^{(2,2)}(p,k)=2J(-\chi_0 f_k^0+\chi_1 e^{-ip}f_k^2),$$

$$g^{(3,0)}(p,k)=[J_\perp+J\{e^{ip}+(1+4\chi_2)e^{-ip}\}]f_k^0-2J\chi_0 f_k^1-2J\chi_0 e^{-ip}f_k^2,$$

$$g^{(3,1)}(p,k)=2J(-\chi_0 f_k^0+\chi_1 e^{ip}f_k^1),$$

$$g^{(3,2)}(p,k)=2J(-\chi_0 e^{-ip}f_k^0+\chi_1 e^{-ip}f_k^2),$$

$$g^{(4,0)}(p,k)=-J_\perp f_k^0+2J\chi_0(1+e^{ip})f_k^1,$$

$$g^{(4,1)}(p,k)=-J(2\chi_1 e^{ip}f_k^1+f_k^2),$$

$$g^{(4,2)}(p,k)=J[2\chi_0(1+e^{-ip})f_k^0-(1+4\chi_2)f_k^1-2\chi_1 e^{-ip}f_k^2],$$

$$g^{(5,0)}(p,k)=g^{(6,0)}(p,k)=2J\chi_1(e^{ip}+e^{-ip})f_k^0,$$

$$g^{(5,1)}(p,k)=g^{(6,1)}(p,k)=-2J\chi_1 f_k^2,$$

$$g^{(5,2)}(p,k)=g^{(6,2)}(p,k)=-2J\chi_1 f_k^1. \quad \text{(B4)}$$

The noninteracting particle-hole propagators b^0 are given as

$$b^0_{\alpha^\dagger\alpha,\alpha\alpha^\dagger}=b^0_{\beta^\dagger\beta,\beta\beta^\dagger}=b^0_{\alpha^\dagger\alpha,\beta\beta^\dagger}=b^0_{\beta^\dagger\beta,\alpha\alpha^\dagger}=\tfrac{1}{4}[g_1^0(p,k,\omega)-g_2^0(p,k,\omega)],$$

$$b^0_{\beta^\dagger\alpha,\alpha\alpha^\dagger}=b^0_{\beta^\dagger\alpha,\beta\beta^\dagger}=\tfrac{1}{4}u_{p+k}^2[g_1^0(p,k,\omega)+g_2^0(p,k,\omega)],$$

$$b^0_{\alpha^\dagger\beta,\alpha\alpha^\dagger}=b^0_{\alpha^\dagger\beta,\beta\beta^\dagger}=\tfrac{1}{4}v_{p+k}^2[g_1^0(p,k,\omega)+g_2^0(p,k,\omega)],$$

$$b^0_{\alpha^\dagger\alpha,\alpha\beta^\dagger}=b^0_{\beta^\dagger\beta,\alpha\beta^\dagger}=-\tfrac{1}{4}u_k^2[g_1^0(p,k,\omega)+g_2^0(p,k,\omega)],$$

$$b^0_{\alpha^\dagger\alpha,\beta\alpha^\dagger}=b^0_{\beta^\dagger\beta,\beta\alpha^\dagger}=-\tfrac{1}{4}v_k^2[g_1^0(p,k,\omega)+g_2^0(p,k,\omega)],$$

$$b^0_{\alpha^\dagger\beta,\alpha\beta^\dagger}=-\tfrac{1}{4}u_k^2v_{p+k}^2[g_1^0(p,k,\omega)-g_2^0(p,k,\omega)],$$

$$b^0_{\beta^\dagger\alpha,\beta\alpha^\dagger}=-\tfrac{1}{4}v_k^2u_{p+k}^2[g_1^0(p,k,\omega)-g_2^0(p,k,\omega)],$$

$$b^0_{\alpha^\dagger\beta,\beta\alpha^\dagger}=-\tfrac{1}{4}v_k^2v_{p+k}^2[g_1^0(p,k,\omega)-g_2^0(p,k,\omega)],$$

$$b^0_{\beta^\dagger\alpha,\alpha\beta^\dagger}=-\tfrac{1}{4}u_k^2u_{p+k}^2[g_1^0(p,k,\omega)-g_2^0(p,k,\omega)], \quad \text{(B5)}$$

with

$$g_1^0(p,k,\omega)=\frac{1}{\omega-\epsilon_k-\epsilon_{p+k}+i\delta},$$

$$g_2^0(p,k,\omega)=\frac{1}{\omega+\epsilon_k+\epsilon_{p+k}-i\delta}. \quad \text{(B6)}$$

Here, χ_0, χ_1, and χ_2 are the bond amplitudes (15), u_k, v_k are the coefficients for the diagonalization (19) of the mean-field Hamiltonian (16), and ϵ_k is the mean-field dispersion (18).

*Present address: Department of Physics, University of Florida, Gainesville, FL 32611.

[1] E. Dagotto and T.M. Rice, Science **271**, 618 (1996).
[2] T.M. Rice, S. Gopalan, and M. Sigrist, Europhys. Lett. **23**, 445 (1993).
[3] M. Azuma, Z. Hiroi, M. Takano, K. Ishida, and Y. Kitaoka, Phys. Rev. Lett. **73**, 3463 (1994).
[4] S. Chakravarty, B.I. Halperin, and D.R. Nelson, Phys. Rev. Lett. **60**, 1057 (1988); Phys. Rev. B **39**, 2344 (1989).
[5] D.V. Khveshchenko, Phys. Rev. B **50**, 380 (1994).
[6] G. Sierra, J. Phys. A **29**, 3299 (1996); in *Lectures Notes in Physics*, Vol. 478, edited by G. Sierra and M.A. Martin-Delgado (Springer-Verlag, Berlin, 1997).
[7] S. Chakravarty, Phys. Rev. Lett. **77**, 4446 (1996).
[8] S. Chakravarty, B.I. Halperin, and D.R. Nelson, Phys. Rev. B **39**, 2344 (1989).
[9] S. Sachdev and R.N. Bhatt, Phys. Rev. B **41**, 9323 (1990).
[10] S. Gopalan, T.M. Rice, and M. Sigrist, Phys. Rev. B **49**, 8901 (1994).
[11] G.S. Uhrig and H.J. Schulz, Phys. Rev. B **54**, R9624 (1996); **58**, 2900(E) (1998).
[12] O.P. Sushkov and V.N. Kotov, Phys. Rev. Lett. **81**, 1941 (1998); V.N. Kotov, O.P. Sushkov, and R. Eder, Phys. Rev. B **59**, 6266 (1999).
[13] S. Trebst, H. Monien, C.J. Hamer, Z. Weihong, and R.R.P. Singh, Phys. Rev. Lett. **85**, 4373 (2000); W. Zheng, C.J. Hamer, R.R.P. Singh, S. Trebst, and H. Monien, Phys. Rev. B **63**, 144410 (2001).

[14] C. Knetter, K.P. Schmidt, M. Grüninger, and G.S. Uhrig, Phys. Rev. Lett. **87**, 167204 (2001).
[15] D.G. Shelton, A.A. Nersesyan, and A.M. Tsvelik, Phys. Rev. B **53**, 8521 (1996).
[16] M. Greiter, Phys. Rev. B **65**, 134443 (2002); **66**, 054505 (2002).
[17] D.C. Johnston, M. Troyer, S. Miyahara, D. Lidsky, K. Ueda, M. Azuma, Z. Hiroi, M. Takano, M. Isobe, Y. Ueda, M.A. Korotin, V.I. Anisimov, A.V. Mahajan, and L.L. Miller, cond-mat/0001147, Phys. Rev. B (to be published).
[18] M. Windt, M. Grüninger, T. Nunner, C. Knetter, K.P. Schmidt, G.S. Uhrig, T. Kopp, A. Freimuth, U. Ammerahl, B. Büchner, and A. Revcolevschi, Phys. Rev. Lett. **87**, 127002 (2001).
[19] T.S. Nunner, P. Brune, T. Kopp, M. Windt, and M. Grüninger, Acta Phys. Pol. B **34**, 1545 (2003).
[20] T.S. Nunner, P. Brune, T. Kopp, M. Windt, and M. Grüninger, Phys. Rev. B **66**, 180404(R) (2002).
[21] P. Jordan and E. Wigner, Z. Phys. **47**, 631 (1928).
[22] More recent discussions of the exploitation of the Jordan-Wigner transformation, in the context of field theories for strongly correlated electron systems, can be found in the following two textbooks: A.M. Tsvelik, *Quantum Field Theory in Condensed Matter Physics* (Cambridge University Press, Cambridge, 1995); E. Fradkin, *Field Theories of Condensed Matter Systems* (Addison-Wesley, Reading, MA, 1991).
[23] X. Dai and Z.B. Su, Phys. Rev. B **57**, 964 (1998).
[24] M. Azzouz, L. Chen, and S. Moukouri, Phys. Rev. B **50**, 6233 (1994).
[25] J. Lorenzana and G.A. Sawatzky, Phys. Rev. Lett. **74**, 1867 (1995); Phys. Rev. B **52**, 9576 (1995).
[26] H. Suzuura, H. Yasuhara, A. Furusaki, N. Nagaosa, and Y. Tokura, Phys. Rev. Lett. **76**, 2579 (1996).
[27] T.D. Kühner and S.R. White, Phys. Rev. B **60**, 335 (1999).
[28] B.M. McCoy, E. Barouch, and D.B. Abraham, Phys. Rev. A **4**, 2331 (1971).
[29] A. Luther and I. Peschel, Phys. Rev. B **12**, 3908 (1975).
[30] Y.R. Wang, Phys. Rev. B **46**, 151 (1992).
[31] T. Yamada, Prog. Theor. Phys. Jpn. **41**, 880 (1969).
[32] J. Lorenzana and R. Eder, Phys. Rev. B **55**, R3358 (1997).
[33] G. Müller, H. Thomas, H. Beck, and J.C. Bonner, Phys. Rev. B **24**, 1429 (1981).
[34] A.H. Bougourzi, M. Couture, and M. Kacir, Phys. Rev. B **54**, R12 669 (1996).
[35] M. Karbach, G. Müller, A.H. Bougourzi, A. Fledderjohann, and K.-H. Mütter, Phys. Rev. B **55**, 12 510 (1997).
[36] Jordan-Wigner transformation in two dimensions: E. Fradkin, Phys. Rev. Lett. **63**, 322 (1989); D. Eliezer and G.W. Semenoff, Phys. Lett. B **286**, 118 (1992); the treatment of two-dimensional systems has recently been reviewed by O. Derzhko, J. Phys. Stud. **5**, 49 (2001).
[37] Jordan-Wigner transformation in three dimensions: L. Huerta and J. Zanelli, Phys. Rev. Lett. **71**, 3622 (1993).
[38] M.A. Martin-Delgado, R. Shankar, and G. Sierra, Phys. Rev. Lett. **77**, 3443 (1996).
[39] D.C. Cabra and M.D. Grynberg, Phys. Rev. Lett. **82**, 1768 (1999).
[40] V.N. Kotov, J. Oitmaa, and Z. Weihong, Phys. Rev. B **59**, 11 377 (1999).
[41] K. Damle and S. Sachdev, Phys. Rev. B **57**, 8307 (1998).
[42] C. Jurecka and W. Brenig, Phys. Rev. B **61**, 14 307 (2000).
[43] M. Grüninger, M. Windt, T. Nunner, C. Knetter, K.P. Schmidt, G.S. Uhrig, T. Kopp, A. Freimuth, U. Ammerahl, B. Büchner, and A. Revcolevschi, J. Phys. Chem. Solids **63**, 2167 (2002).
[44] P.J. Freitas and R.R.P. Singh, Phys. Rev. B **62**, 14 113 (2000).
[45] K.P. Schmidt, C. Knetter, and G.S. Uhrig, Europhys. Lett. **56**, 877 (2001).